

«

»

1.6.17 –

-

-

– 2022

	4
1	16
1.1	16
1.2	23
1.2.1	23
1.2.2	AERONET-OC	25
1.3	,	26
1.4	31
1.4.1	(1994)	36
	1	41
2	43
2.1	43
2.2	48
2.3	SeaBASS	50
	2.....	52
3	53
3.1	<i>in situ</i> AERONET	53

3.2

. 57

3..... 66

4

..... 68

4.1

..... 68

4.2.

,
..... 76

4.3

..... 86

4.4

Rrs *in situ*

..... 95

4..... 98

..... 99

..... 102

..... 105

[Morel et al., 1977; Gordon et al., 1994; , 2017]. $L_w()$

[Shettle et al. 1979; Ahmad et al., 2010; Dubovik et al., 2000; Jamet et al., 2004]. ,

MODIS-Aqua, (L_{TOA}) , [Gordon, 1978; (Ruddick et al., 2000; Moore et al., 1999; Siegel et al., 2000; Stumpf et al., 2003; Bailey et al., 2010)]. L_w ,

g L_{TOA} [Gao et al., 2000; Wang and Shi, 2007; Oo et al., 2008; Wang et al., 2009 Land and Haigh, 1997; Chomko and Gordon, 1998; Stamnes et al., 2003; Kuchinke et al., 2009; Shi et al., 2016].

10–15 %

L_w TOA

5% -

(CDOM)

[., 2017; Morel et al, 1979].

, (1989)

L_{wn} ,

$L_w()$

[Gordon, 1989].

$L_{wn}()$

,

$Rrs()$,

.

in situ

,

.

,

λ

$$k = 2\pi/\lambda.$$

k

,

[Moulin, C et al., 2001; . . . 1992; . . .

.,2004; . . ., 2009; Shibanov E.B. et al., 2008].

,

[IOCCG (2006).; IOCCG

(2007).; IOCCG (2008).; IOCCG (2010).; IOCCG (2012); IOCCG (2014)],

,

,

:

1.

-

[. . . , 2004; . . . , 2009; . . . , 2022];

2.

(,) [Frouin et al., 2014];

3.

(,) [. . . , 2002; Shybanov et al., 2021; . . . , 2021; Suslin et al., 2016; Kalinskaya et al., 2022].

,

,

.

,

,

,

.

,

.

.

.

,

,

.

,

.

,

[Gordon et

al., 1997; Chomko et al., 1998; Antoine et al., 1999].

CALIOP

(CALIPSO) [Kim et al., 2018; Omar et al., 2009].

CALIPSO

,

L_{wn} -

,

,

,

.

—

,

.

1.

.

2.

,

AERONET-OC.

3.

,

NASA.

4.

.

—

«

».

OC. : MODIS-Aqua/Terra AERONET-
 Python.
 SeaDAS.

1.

$\lambda-4.$

2.

AERONET-OC,

$\lambda-3,6.$

3.

AERONET-OC.

CI (412/443)

1.

2.

3.

AERONET-OC,
NASA.

1. “ : , , ”.
 , 27-30 2022.
2. “ : , , ”.
 , 3-7 2017.
3. XXVIII " .
 ",04-08 , 2022.
4. XXVII C “ .
 ”,05-09 , 2021.
5. XXVI « .
 », , 6-10 2020.
6. XXV « .
 », , 1-5 2019.

7. XXV - “
” . , 18-22 2017.
8. III «
», , 21-25 2018.
9. " " , 12-16
2018.
10. International multidisciplinary scientific geoconference surveying geology and mining ecology management, SGEM. Bulgaria, 2019.
11. X "
".
 . - , 9-11 2019.
12. V «
» . , 21-25 2020.
17 ,
: 8 ,
 ,
«SCOPUS» «Web of Science» [1–8]. 6
 ,
«SCOPUS» «Web of Science» [Kalinskaya et al., 2018; Kalinskaya et al., 2020; Papkova et al., 2022; Papkova et al., 2020; Papkova et al., 2021; Kalinskaya et al., 2021].

1. Kalinskaya D.V., Varenik A.V., **Papkova A.S.** Phosphorus and silicon as markers of dust aerosol transfer over the Black Sea region // *Sovremennye Problemy Distantionnogo Zondirovaniya Zemli iz Kosmosa*. – 2018. – V. 15, 3. – P. 217-225. DOI: 10.21046/2070-7401-2018-15-3-217-225.

2. **Papkova A.S.**, Papkov S.O., Shukalo D.M. CALIPSO stratification of atmospheric aerosols with environmental assessment of dust content over the

Black Sea region // *Sovremennye Problemy Distantcionnogo Zondirovaniya Zemli iz Kosmosa*. – 2020. – V. 17, 1. – P. 234-242. DOI: 10.21046/2070-7401-2020-17-1-234-242.

3. Kalinskaya D.V., **Papkova A.S.**, Kabanov D.M. Research of the Aerosol Optical and Microphysical Characteristics of the Atmosphere over the Black Sea Region by the FIRMS System during the Forest Fires in 2018–2019 // *Physical Oceanography*. – 2020. – V. 27, 5. – P. 514-524. DOI: 10.22449/1573-160X-2020-5-514-524.

4. Kalinskaya, D.V., **Papkova, A.S.**, Varenik, A.V. The case of absorbing aerosol anomalous transport over the Black Sea in the spring of 2020 // *Sovremennye Problemy Distantcionnogo Zondirovaniya Zemli iz Kosmosa*. – 2021. – V. 18, 2. – P. 287-298. DOI: 10.21046/2070-7401-2021-18-2-287-298.

5. **Papkova A.**, Papkov S., Shukalo D. Prediction of the Atmospheric Dustiness over the Black Sea Region Using the WRF-Chem Model // *Fluids*. – 2021. – V.6, 6. – P. 201. DOI: 10.3390/fluids6060201.

6. **Papkova A.S.**, Shybanov E.B. Influence of dust aerosol on the results of atmospheric correction of remote sensing reflection of the Black and Mediterranean Seas from MODIS satellite data // *Sovremennye Problemy Distantcionnogo Zondirovaniya Zemli iz Kosmosa*. – 2021. – V. 18, 6. – P. 46–56. DOI: 10.21046/2070-7401-2021-18-6-46-56.

7. Kalinskaya D.V., **Papkova A.S.** Why Is It Important to Consider Dust Aerosol in the Sevastopol and Black Sea Region during Remote Sensing Tasks? A Case Study // *Remote Sensing*. – 2022. – V.14, 8. – P. 1890. DOI: 10.3390/rs14081890.

8. Shybanov E.B. **Papkova A.S.** 2022. Algorithm for Additional Correction of Remote Sensing Reflectance in the Presence of Absorbing Aerosol: Case Study // *Physical Oceanography*. – 2022. – 29(6). – P. 688-706. DOI:10.22449/1573-160X-2022-6-688-706

« »

:

– «

» («

»), 0827-2019-0002, ;

– «

» («

»), FNNN-2021-0003, .

– ()

19-35-90066 ().

.. ,

.

AERONET-OC.

.

,

:

in situ

,

.

..

AERONET-OC.

24

12

.

111

.

,

.

,

.

,

.

,

.

,

.

.

1

1.1

$$L_w(\lambda),$$

[., 1953; Mobley, 2002].

(z)

$$\begin{aligned} \mu \cdot \frac{dL(z, \mu, \varphi)}{dz} &= -c(z) \cdot L(z, \mu, \varphi) + \\ &+ \frac{b(z)}{4 \cdot \pi} \cdot \int_0^{2\pi} \int_{-1}^1 L(z, \mu', \varphi') \cdot p(z, \mu, \varphi, \mu', \varphi') \partial \mu' \partial \varphi' + J(z, \mu, \varphi), \end{aligned} \tag{1.1}$$

$$c(z) = a(z) + b(z),$$

$$L(z, \mu, \varphi) -$$

μ φ z
();

$$c(z) - b(z) - ;$$

$$a(z) - ;$$

$$p(z, \mu, \varphi) - .$$

$$\int_0^{2\pi} \int_0^\pi p(z, \cos(\gamma), \varphi) \cdot \sin(\gamma) \cdot \partial \gamma \cdot \partial \varphi = 4 \cdot \pi, \tag{1.2}$$

$\gamma -$

$$\cos(\gamma) = \mu \cdot \mu' + \sqrt{(1 - \mu^2) \cdot (1 - \mu'^2)} \cdot \cos(\varphi - \varphi'), \quad (1.3)$$

$\mu, \mu' -$

;

$\varphi, \varphi' -$

$$(1.1) \quad J(z, \mu, \varphi)$$

$$J(z, \mu, \varphi) = \frac{b(z) \cdot p(z, \mu, \varphi, \mu_0, \varphi_0)}{4\pi} \cdot S_0 \cdot \exp\left[-\frac{1}{\mu_0} \int_0^z c(x) \cdot dx\right], \quad (1.4)$$

$S_0 -$

(

).

$$\tau = \int_0^z c(x) \cdot dx -$$

$z.$

z

(1.1)

$$\begin{aligned} \mu \frac{dL(\tau, \mu, \varphi)}{d\tau} &= -L(\tau, \mu, \varphi) + \\ &\frac{\omega}{4 \cdot \pi} \cdot \int_0^{2\pi} \int_{-1}^1 p(\mu, \varphi, \mu', \varphi') L(\tau, \mu', \varphi') d\mu' d\varphi' + \\ &\frac{\omega \cdot p(\mu, \varphi, \mu_0, \varphi_0) S_0}{4\pi} \cdot \exp\left[-\frac{\tau_0 - \tau}{\mu_0}\right], \end{aligned}$$

$$\omega = \frac{b}{a+b} - \quad ($$

).

τ

$\tau_0,$

[Philpot, 1987]

$$L(0, \mu, \varphi) = \frac{S_0 \omega}{4\pi} \frac{p(\mu_0 \rightarrow \mu, \varphi_0 \rightarrow \varphi)}{1 - \frac{\mu}{\mu_0}} \left\{ 1 - \exp \left[-\tau_0 \left(\frac{1}{\mu_0} - \frac{1}{\mu} \right) \right] \right\}, \mu < 0. \quad (1.5)$$

($L(z, \mu, \varphi)$) .

, $L(z, \mu, \varphi)$

$(\mu, \varphi, \mu', \varphi')$,

$$L_1(\tau, \mu_0, \mu) = \omega \frac{\mu_0 \cdot S_0 \cdot p(\mu_0, \mu)}{4 \cdot \pi \cdot (\mu_0 - \mu)} \cdot \left[\exp\left(-\frac{\tau}{\mu_0}\right) - \exp\left(-\frac{\tau}{\mu}\right) \right],$$

$$L_1(\tau, \mu_0, -\mu) = \omega \frac{\mu_0 \cdot S_0 \cdot p(\mu_0, -\mu)}{4 \cdot \pi \cdot (\mu_0 + \mu)} \cdot \left[\exp\left(-\frac{\tau}{\mu_0}\right) - \exp\left(-\frac{\tau_0}{\mu_0} - \frac{\tau_0}{\mu} + \frac{\tau}{\mu}\right) \right],$$

$\tau_0 -$

;

$p(\mu_0, -\mu) -$

$$\frac{\tau_0}{\mu} \quad \frac{\tau_0}{\mu_0},$$

$(\tau = 0)$

$(\tau = \tau_0)$

$$L_1(\tau, \mu_0, \mu) = \omega \frac{S_0 \cdot p(\mu_0, \mu)}{4\pi\mu} \cdot \tau_0,$$

$$L_1(\tau, \mu_0, -\mu) = \omega \frac{S_0 \cdot p(\mu_0, -\mu)}{4\pi\mu} \cdot \tau_0.$$

[Viollier et al.,

1980]

(1.5).

, $p(\mu_0, -\mu) < 1$

$$\mu \frac{dL(z, \mu, \varphi)}{dz} = \beta(z, \mu, \mu_0, \varphi) \cdot S_0, \quad (1.6)$$

$$\beta(z, \mu, \mu_0, \varphi) - , \quad \frac{p(\mu, \mu_0)}{4\pi} b(z) .$$

$z=0$ (z) [, 2018].

$$\mu \frac{dL}{dz} = -cL + \frac{b}{2} \int_{-1}^1 p(\mu, \mu') L(z, \mu') d\mu'. \quad (1.7)$$

(1.7) μ $[-1,0]$ $[0,1]$,

E

E

$$\frac{\partial E \downarrow}{\partial z} = \frac{a + b\varphi_1}{\mu_1} E \downarrow + \frac{b\varphi_2}{\mu_2} E \uparrow,$$

$$\frac{\partial E \uparrow}{\partial z} = \frac{a + b\varphi_2}{\mu_2} E \uparrow + \frac{b\varphi_1}{\mu_1} E \downarrow,$$

$$\varphi_1 = \frac{1}{2} \int_0^1 L\mu d\mu \int_{-1}^0 p(\mu, \mu') d\mu' / \int_0^1 Ld\mu,$$

$$\varphi_2 = \frac{1}{2} \int_{-1}^0 L\mu d\mu \int_0^1 p(\mu, \mu') d\mu' / \int_{-1}^0 Ld\mu,$$

μ_1^-

;

μ_2^-

.

μ φ .

$\mu_i(z)$ $\varphi_i(z)$

$\mu_i \quad \varphi_i$

R

[, 1978]

$$\frac{(1 - R_\infty)^2}{2R_\infty} = \frac{a}{b\varphi}.$$

()

$$R_\infty \sim \frac{b_b(\lambda)}{a(\lambda) + b_b(\lambda)}.$$

$$x = \frac{b_b(\lambda)}{a(\lambda) + b_b(\lambda)}$$

$\rho(\lambda)$

$:\rho(\lambda) = \pi L_u(\lambda, 0-) / E_d(\lambda, 0-), \quad L_u(\lambda, 0-)$

$E_d(\lambda, 0-) -$

$$\rho = \frac{T \uparrow \cdot T \downarrow}{m^2} R_\infty,$$

$m -$;
 $-$.
 ,

[Morel et al., 1995]

$$L_w(\theta_s, \theta_v, \phi, \lambda, W, a, b_b) = E_d(\theta_s, \lambda) \cdot R(\theta_s, \theta_v, W) \cdot \frac{f(\theta_s, \lambda, W, a, b_b)}{Q(\theta_s, \theta_v, \phi, \lambda, W, a, b_b)} \cdot \frac{b_b(\lambda)}{a(\lambda) + b_b(\lambda)},$$

$f -$,

($a - b_b$);

$Q -$, sr^{-1} ;

$v -$;

$-$,

$s -$,

$W -$ ().

$L_w,$

, ($v -$),

(s), (W)

. , E_d

, s . f/Q

0,09 0,11

().

, [Gordon, 1989]

L_{wn} , $L_w(\lambda)$ (1.1)

$$L_{wn}(\lambda) = \frac{L_w(\lambda)}{t_0(\lambda) \cos \theta_0},$$

 $t_0(\lambda)$ —

;

 $0 -$

.

.

1.2

1.2.1

c

-

.

,

.

,

.

,

,

.

,

 $L_w(\lambda)$ « »

10–15 %

,

.

,

,

«

»

 $L_w(\lambda)$

5% -

[Morel et al., 1977].

$$L_w(\lambda)$$

$$L_w$$

«

»,

$$L_{TOA}$$

Ocean Color

(L_{TOA}) [Gordon et al., 1994].

$$L_{TOA}$$

$$L_{TOA}(\lambda) = [L_r(\lambda) + L_a(\lambda) + t_{dv}(\lambda)L_f(\lambda) + t_{dv}(\lambda)L_w(\lambda)]t_{gv}(\lambda)t_{gs}(\lambda)f_p(\lambda), \quad (1.8)$$

$$L_r(\lambda) -$$

;

$$L_a(\lambda) -$$

,

;

$$L_f(\lambda) -$$

;

$$L_w(\lambda) -$$

;

$$t_{dv}(\lambda) -$$

;

$$t_{ds}(\lambda) -$$

;

$$t_{gv}(\lambda) -$$

-

,

;

$$t_{gs}(\lambda) -$$

;

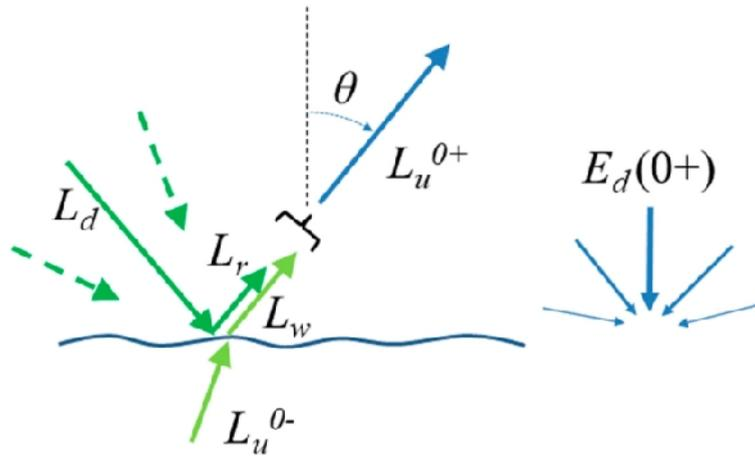
$f_p(\lambda) -$

1.2.2

AERONET-OC

(, .).

1.1.



1.1 -

(L_w).

1.1 L_u^{0-} L_u^{0+} -

, L_r - (), L_d - () ; E_d -

1.1

,

$$L_w = L_u^{0+} - L_r,$$

$L_{sky}(\lambda) -$

,

,

$L_w(\lambda)$

$$L_w(\lambda) = L_u^{0+}(\lambda) - R_f(\lambda) \cdot L_{sky}(\lambda), \tag{1.9}$$

$$R_f - \quad . \quad (1.9)$$

[Ruddick et al., 2019].

R_f

[Zibordi et al., 2009] .

$L_w(\lambda)$

$L_s(\lambda)$

$L_q(\lambda)$.

2 .

[, 2001].

1.3

[Sosik et al., 1995], $a(\lambda)$

(1.10)

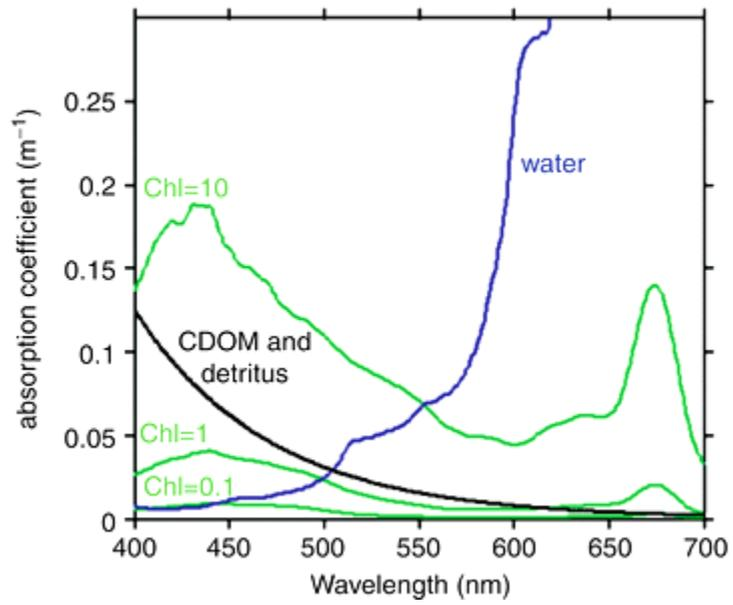
$$a(\lambda) = a_w(\lambda) + a_{ph}(\lambda) + a_d(\lambda) + a_{dm}(\lambda), \quad (1.10)$$

λ ;
 $a_w(\lambda)$ [Smith, 1981];
 $a_d(\lambda)$;
 $a_{ph}(\lambda)$;
 $a_{dm}(\lambda)$;

$$a(\lambda) = a_w(\lambda) + a_{ph}(\lambda) + a_{ddm}(\lambda), \quad (1.11)$$

$a_{ddm}(\lambda)$.

1.2.



1.2 –

0,1; 1 10 ⁻³.

1.2

550

, CDOM,

0,2

CDOM,

$$a_{ph}(\lambda)$$

(1.12)

C_{chl}

$$a_{ph}(\lambda) = C_{chl} \cdot a_{ph}^{spe}(\lambda) \tag{1.12}$$

,

$$a_{ph}^{spe}(\lambda)$$

,

$$a_{ph}^{spe}(\lambda) \quad C_{chl}$$

(b_b)

,

[Morel , 1977]

$$b_b(\lambda) = b_{bw}(\lambda) + b_{na}(\lambda) + b_{ba}(\lambda), \quad (1.13)$$

$$b_{bw}(\lambda) -$$

;

$$b_{ba}(\lambda), b_{bna}(\lambda) -$$

.

,

.

,

.

.

1.1,

$$\rho(\lambda) = k \cdot b_b(\lambda) / a(\lambda)$$

k

,

.

0,17 [.., 2003].

k

0,1 0,17.

,

,

,

(1.14)[.., 2005]

$$\rho(\lambda) = k \frac{b_{bw}(\lambda) + b_{bp}(\lambda_0) \left(\frac{\lambda}{\lambda_0}\right)^\gamma}{a_w(\lambda) + C_{chl} \cdot a_{chl}(\lambda) + C_{ddm} e^{-\alpha(\lambda-\lambda_0)}}, \quad (1.14)$$

$k = 0,15$ [.., 2008];

b_{bw} – ;

v – ,

;

a_w – ;

a_{chl} – [Bricaud

et al., 1995];

α – ;

b_{bp} – λ_0 ;

C_{chl} – ;

C_{ddm} – .

C_{chl} C_{ddm}

.

.

[.., 2009] ,

-

,

(1.15)

$$\rho(\lambda) = k \frac{b_{bw}(\lambda) + b_{bp}(\lambda_0) \left(\frac{\lambda}{\lambda_0}\right)^\gamma}{a_w(\lambda) + C_{ddm} e^{-\alpha(\lambda-\lambda_0)}}. \quad (1.15)$$

2004].

1.4

CZ S (Costal Zone Color Scanner),

[Werdell et al., 2002]

420–440

[

..

«

–

».

670

750

,

«

»

LOWTRAN-6

0,35–40

[4].

(RH).

1972]

[Junge,
[Deirmendjian, 1964]

—

[Davies, 1974]

(Ocean Color

SF79) [Shettle et al., 1976]

:

(urban),

(rural),

(maritime)

(RH).

LOWTRAN (LOW spectral atmospheric TRANsmission)

$$n(r) = \frac{dN(r)}{dr} = \sum_{i=1}^2 \left(\frac{N_i}{\ln(10)r\sigma_i\sqrt{2\pi}} \right) \exp\left[-\frac{(\log r - \log r_i)^2}{2\sigma_i^2} \right], \quad (1.16)$$

$N(r)$ — r ;

σ_i — ;

r_i — ;

N_i — r_i .

[Whitby et al., 1975]

(Maritime) , (Rural), (Urban) ,
,

RH.

Ocean Color

1.1.

AERONET

(Aerosol ROboties NETwork)

CIMEL-318.

1.1 –

	SSA (865)	(g)	(AE) (510,865)
*	1,0	0,724–0,840	–0,087—0,016
*	0,98–0,99	0,69–0,82	0,09–0,5
**	0,97–0,99	0,68–0,81	0,23–0,76
*	0,93–0,99	0,603–0,76	1,19–1,53
*	0,6–0,94	0,63–0,77	0,85–1,14
**	0,83–0,99	0,66–0,76	0,29–0,36

*_ SF79;*_ (1994);

CIMELS

Ocean Color (2009)

[Ahmad et al., 2010].

(ω)

AERONET.

(RH)

. [Ahmad et al., 2010]

[Häne et al., 1976]

SF79

(m)

. (r_f r_c)

RH 30% 95%.

RH

$$r(a_w) = r_0 \left[1 + \rho \frac{m_w \cdot a_w}{m_0} \right]^3, \tag{1.17}$$

a_w — , RH
 ;
 r_0 — $RH = 0$;
 m_0 — ;
 m_w — RH ;
 —
 .
 [Häne et al., 1976]
 $m_w = m_0$ RH ,
 20% 99%. . [Ahmad et al., 2010]
 ,
 , RH
 NCEP
 [Werdell et al., 2002]. -
 ,
 .
 ,
 SF79.
 , (70%) ,
 (30%) ,
 . [Ahmad et al., 2010]
 SF79 ,
 RH 30%
 95%

$$n = n_w + (n_0 - n_w) \left[\frac{r_0}{r_{rh}} \right]^3, \tag{1.18}$$

n_w – ;
 n_0 – $RH=0$;
 r_0 – $RH=0$;
 r_{rh} – RH .

, Ocean Color
 GW94 [Gordon et al., 1994] ,
 [Bailey et al., 2006]
 . NASA
 LUT (Lookup table)
 SF79LUT. LUT
 – .
 (IFOV).

1.4.1 (1994) .

[Gordon et al., 1994].
 ()
 (, 748 869 MODIS (. Moderate Resolution
 Imaging Spectroradiometer)),

, [IOCCG (2000)].
 , Gordon

$$\varepsilon(\lambda_i, \lambda_j), \quad \lambda_i, \lambda_j$$

$$\varepsilon(\lambda_{IR1}, \lambda_{IR2})$$

λ_{IR2} , $\varepsilon(\lambda_{IR1},$
 $\lambda_{IR2}), \lambda_{IR1}, \lambda_{IR2} -$ $\varepsilon_{\text{mod}}(\lambda_{IR1},$
 $-$.
 ,

[, 2004]. ,

() [, 2004],

ε

412 443 ,

A(),

λ

Rrs(412)

, [, 2004].

, [, 2004].

$$Rrs(\lambda)_m = C_1 + C_2 \lambda^{-2}$$

level 2

SeaWiFS.

[, 2004].

1976].

[,

(SMA)

SOA [Gordon et al, 1997; Chomko et al., 1998].

[Antoine et al., 1999]

MERIS

510 705

(,)

510 .

Rrs(510)

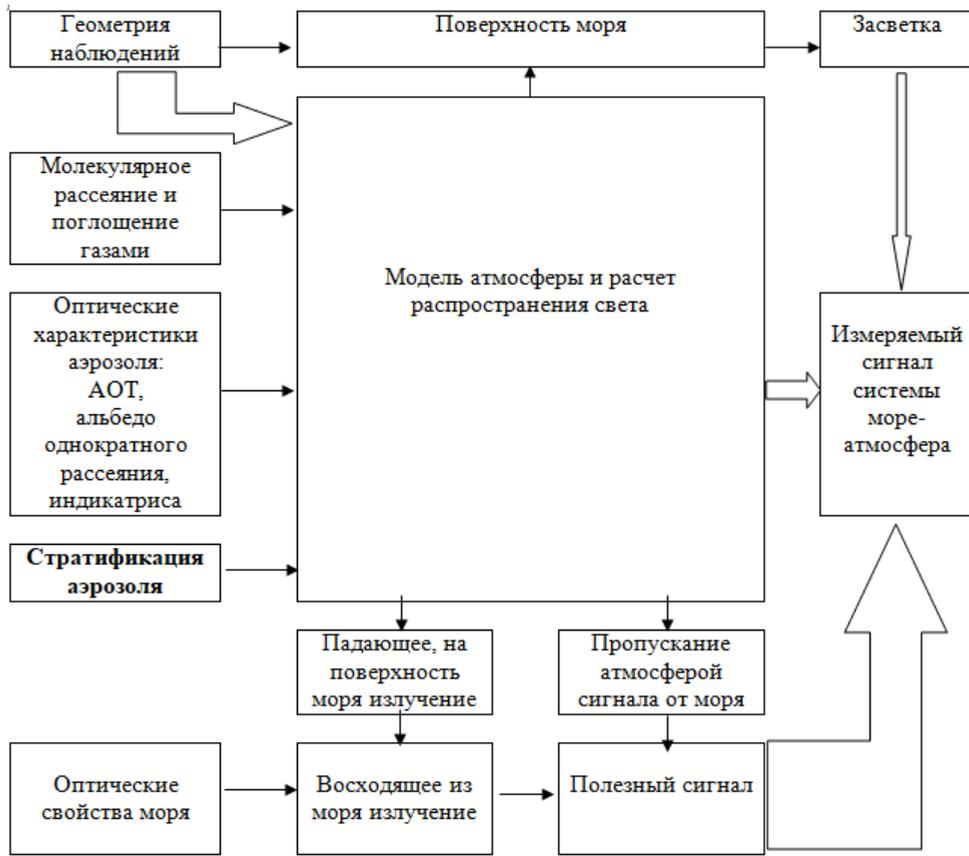
(

)

Case 1.

– (1.3).

« »



1.3 – –

1

$R_{rs}(\lambda)$,

in situ

λ

$$k=2\pi/\lambda.$$

k

- ,
- .
- ,
- .
- :
1. — [. . . ., 2004;, 2009;, 2022];
 2. (,) [Frouin et al., 2014];
 3. (,) [. . . ., 2002; Shybanov et al., 2021;, 2021; Suslin et al., 2016; Kalinskaya et al., 2022].

412–443 ,

[Gordon et al., 1997; Chomko et al., 1998; Antoine et al., 1999].

2.1

, *in situ*

() AERONET (Aerosol ROboties NETwork) [42].

Cimel-318 (CE-318).

).

340, 380, 440, 500, 670, 870, 940 1020

()

(GSFC NASA)

[Holben et al., 1998].

AERONET

(

;

);

(

,

,

);

[Dubovik et al., 2000; Dubovik et al., 2000a].

AERONET

: Sevastopol (44,616N, 33,517E), Gloria (44,600N, 29,360E) (2019 Section_7), Galata_Platform (Galata) (43,045N, 28,193E) Eforie (44,075N, 28,632E). Sevastopol

2015 . (2.1).



2.1 – AERONET

Gloria AERONET-OC, 2010

12 ..

40 Galata

AERONET-OC, 2014 13

35 .

AERONET,

AERONET Ocean Color

(AERONET-OC)

. AERONET-OC

,)

,)

,)

Section-

7(Gloria) Galata,

(L_w),

(L_{wn})

. [Zibordi et al., 2009]

L_w.

L_{wn}()

Rrs()

F_o()

[Thuillier et al., 2003].

Galata Gloria

400, 412, 443, 490, 510, 560, 620, 667, 779, 865 1020 .

:

(AE)

AERONET: Sevastopol

2006

2014

Gloria

2014

2018 .

10759 .

7-

AERONET

«

+

(

/

)».

118-

98

20 .

(

), 1 ,
 . , 21 (21
)
 [, 2020]. *AOT*
 () 2.1.

2.1 – *in situ*

	<i>AOT</i> ₁₀₂₀	<i>AOT</i> ₈₇₀	<i>AOT</i> ₆₇₅	<i>AOT</i> ₅₀₀	<i>AOT</i> ₄₄₀
	0.131±0.06	0.146±0.06	0.176±0.07	0.237±0.08	0.264±0.09
	0.072±0.03	0.087±0.04	0.121±0.05	0.19±0.07	0.22±0.08

2.1
 ,
 ,
 .
 .
 1,5–2 . 440–870
 () [Basart et al., 2009].
 , AE (0.75) [Gkikas et al., 2021].
 , – [Lee et al., 2017].

7-

).
NASA (Goddard Code 614 — The Atmospheric Chemistry and
Dynamics Branch (T. Kucsera)).

7-
(00Z 12Z)

(950 , 850 , 700 500)

AERONET

0,5, 1,5, 3 5 . 4
, 4 (400, 300, 250 200
) , 7, 9, 10 12 [Schoeberl et al.,
1995]. ,

7- AERONET

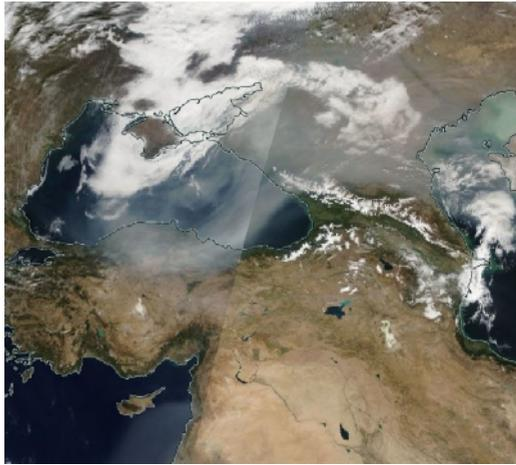
(, ,
.)

. , 19.10.2017
(2.2 ()) 16.10.2018 (2.2 ())

MODIS-Aqua

(
2.2 (,)) , 702 (19.10.2017) 906 (16.10.2018)

[., 2015].

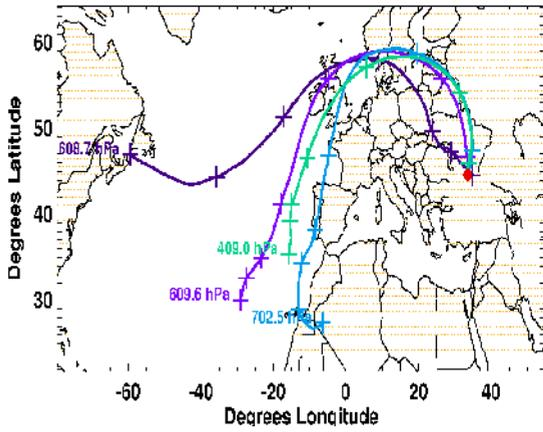


()



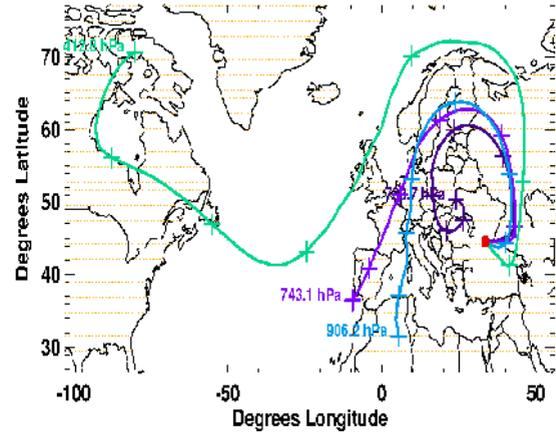
()

Starting Location Station (red dot): Sevastopol
7-Day Back-Trajectories: kinematic, 2017-10-19



()

Starting Location Station (red dot): Sevastopol
7-Day Back-Trajectories: kinematic, 2018-10-16



()

2.2 –

MODIS-Aqua () 19.10.2017;

() 16.10.2018 7-

() 19.10.2017; () 16.10.2018

2.2

MODIS-Terra MODIS-Aqua

36

9

673–683

MODIS

36

0,4 14,4 . 1-2 250 ,
3-7 - 500 , (8-36) - 1000 .
2330 () 10

;

(reprocessing),

NASA 2009-2011 .

(<https://oceancolor.gsfc.nasa.gov>),

12,

1, 3-4,

1 .

MODIS

44

,

,

,

:

,

,

,

,

,

:

level 2 - 1 , level 3 -

(

,

,

).

2.2

,

MODIS

[O'Reilly et al., 1998].

2.2 –

MODIS	Aqua	2330	250/500 /1000	36	405–14385
MODIS	Terra	2330	250/500 /1000	36	405–14385
VIIRS	SuomiNPP	3000	375/750	22	402–11800
VIIRS	JPSS–1	3000	375/750	22	402–11800

$Rrs(\lambda)$ (sr^{-1}),
 MODIS 412, 443, 469, 488, 531, 547,
 555, 645, 667, 678 .
 MODIS $Rrs(\lambda)$ 2–4
 440–670 . MODIS-Aqua
 869 . (AE)
 443 865 .
 (),
 Ocean Color MODIS-Aqua
 .
 ,
 AOT [, 2012].

2.3 SeaBASS

SeaBASS MODIS-Aqua
 AERONET. SeaBASS (SeaWiFS Bio-optical Archive and

Storage System)

in situ,
[IOCCG (2000)].

±3

(BRDF)

Rrs in situ

« »

[Morel et al., 1995].

(5 × 5),

in situ.

(,).

SeaBASS

: (LAND),

(STRAYLIGHT, HIGLINT, HILT, ATMWAR), LOWLW ($L_w(555) < 0,15$)

(NAVFAILE),

(CLDICE).

in situ

±3

Rrs()

[O'Reilly et al., 2019].

531, 547 555 *in situ*
510 560 SeaBASS

2

(MODIS-Aqua),

(AERONET-OC),
(AERONET).

7-

AERONET (*Goddard Code 614*),

MODIS-Aqua

(, ,).

[, 2020;

Kalinskaya et al., 2022; Papkova et al., 2022]

3

3.1 *in situ* AERONET

($L_{wn}(\lambda)$)

AERONET-OC,

Ocean Color $L_{wn}(\lambda)$

$Rrs(\lambda)$.

AERONET-OC.

$Rrs(\lambda)$

SeaBASS: 2

AERONET

(Gloria, Galata)

Venise (

).

,

AERONET-OC

$Rrs(\lambda)$.

Gloria, Galata Venise SeaBass

MODIS-

Aqua - 4580

, -

$Rrs(\lambda)$

$Rrs(\lambda)$

-

() 838 . 190
 – Galata, 239 – Gloria, 409 – Venise.

in situ Rrs() AERONET

$$\rho(\lambda) = f(b_b(\lambda)/a(\lambda)). \tag{3.1}$$

$\rho(\lambda)$

$$b_b(\lambda) = 2\pi \cdot \int_{90}^{180} \beta(\lambda, \theta) \cdot \sin \theta \cdot d\theta$$

$a(\lambda)$

[Morel A et al., 1977]

$$\rho(\lambda) = k \cdot b_b(\lambda)/a(\lambda) \tag{3.2}$$

(3.2)

k . $k=0,15$ [Bricaud et al.,

1995].

1.3

AERONET-OC

$$\rho(\lambda) = k \frac{b_{bw}(\lambda) + b_{bp}(\lambda_0) \left(\frac{\lambda}{\lambda_0}\right)^\gamma}{a_w(\lambda) + C_{chl} \cdot a_{chl}^*(\lambda) + C_{ddm} e^{-\alpha(\lambda-\lambda_0)}}, \quad (3.3)$$

b_{bw} – ;
 $b_{bp}(\lambda_0)$ – ;
 γ – ;
 $a_w(\lambda)$ – ;
 C_{chl} – ;
 $a_{chl}^*(\lambda)$ – ,
 [, 2009]
 $C_{chl} = 0.75 / \text{ }^3$ [, 2004];
 α – ;
 C_{ddm} – ,
 .

(0,0015), , $\gamma = 1$.

AERONET ,

3.3,

$$f = \sum_{\lambda_i} [\rho_{\text{exp}}(\lambda_i) - \rho_m(\lambda_i)]^2 \approx f_m = \sum_{\lambda_i} \rho_{\text{exp}}^2(\lambda_i) \cdot [1/\rho_{\text{exp}}(\lambda_i) - 1/\rho_m(\lambda_i)]^2, \quad (3.4)$$

$$\rho_{\text{exp}}(\lambda_i) - \lambda_i ;$$

$$\rho_m(\lambda_i) - \lambda_i .$$

() ,

,

· ,

,

« »

·

·

·

,

in situ

Rrs()

$$\frac{2\sigma}{\max(Rrs(\lambda))} .$$

,

·

in situ

,

,

– 0,0505;

–

0,0449.

, 838

,

659

,

21%

. 327

Venise, 176

Gloria 156

Galata.

,

,

21% *in situ*

Rrs()

, [, 2022]. , (, ,).

3.2

•

Gloria Galata_Platform AERONET 2
) 2011 2022 1,5 (

— $Rrs()$: , ,

[IOCCG (2000); Balch et al., 2011].

, $Rrs()$ $L_{wn}()$ [Müller et al., 2019; Iglesias-Rodríguez et al., 2002]. $Rrs()$

PIC [Mitchell et al., 2017; Balch et al., 2018].

(CZCS)
 (SeaWiFS) [Brown

et al., 1994; Kopelevich et al, 2014].

SeaWiFS 1998–2002 .

[Mikaelyan et al., 2005; Mikaelyan et al., 2011; Kubryakov et al., 2019].

3.1 [Lobkov, 2017].

3.1 – (. . ⁻¹)

2005–2013 .

			–	
	220.50	392.4	0	390.3
	83.54	127.8	2628.93	3.04
	46.10	15.85	14.7	1.15
	287.50	24.90	3.4	0.5

AERONET–

OC (. . Galata_Platform Gloria/Section –7)

[Zibordi et al., 2015]

: , ,

1991 2008 ,

[Stagl et al., 2015].

(Galata-8841 Gloria-7171),

,

412

10%.

,

.

,

42 % ,

.

— ,

,

,

.

Rrs()

Galata

553

2013

2021 ,

Gloria 408

2011

2019 .

,

961

Rrs()

10

K-Means.

«K

».

(K)

(

6

).

,

.

,

,

K-

means

.

AERONET

3.2.

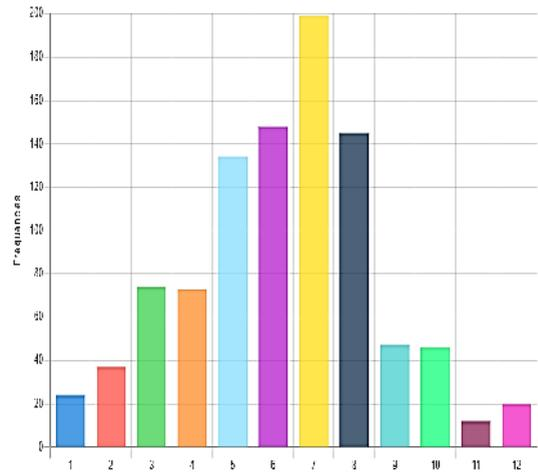
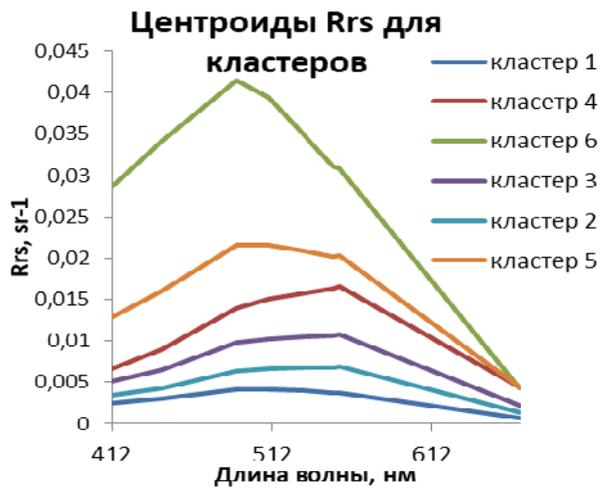
3.2 –

AERONET

	Gloria	Galata_Platform
	44	61
	36	46
	106	176
	222	270

6

(3.1).



()

()

3.1 –

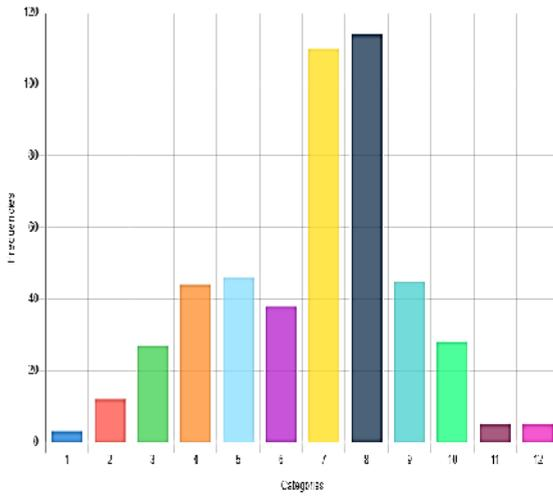
Rrs()

6

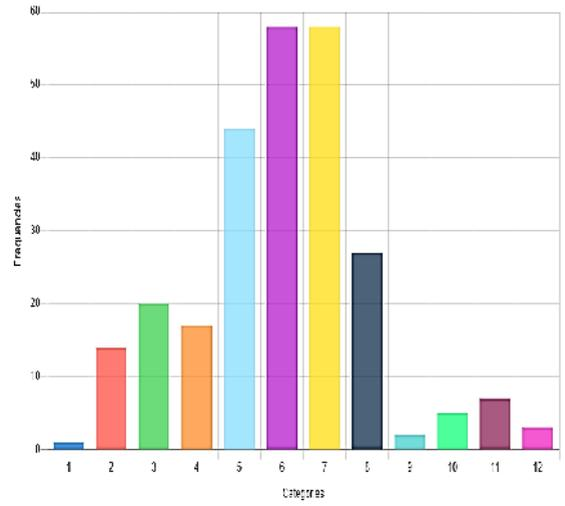
()

().

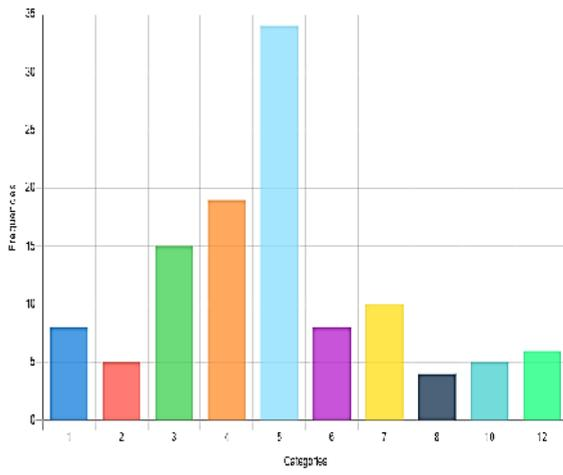
3.2,



1

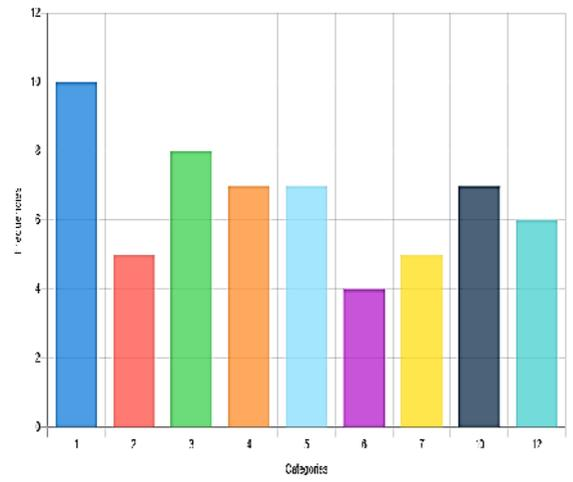


2



3

3.2 –



4

1-4

477,

49%

490

(3.2 ()).
 « » ()
)

412

Rrs()

0,0016.

Rrs()

256

27%

555

(3.2 ()).

117

(12%

),

Rrs()

2

555

(

).

(

3.2 (),

Gloria AERONET-OC,

12

59

(6%).

Rrs()

555

(

3.2 ().

(

).

5

44

(5%),

6

6

(0,6

%).

(3.1)

6

412

 $Rrs()$

0,009.

 $Rrs()$

« »

 $Rrs()$

4

5 6

Ocean Color

- (3.3).

 $Chl-a$

[Hu et al, 2012; Hu et al,

2019].

3.3 –

AERONET (Galata, Gloria)

	$CI(412/443)$	$CI(443/555)$	$CI(443/488)$	$CI(443/547)$
1	$0,83\pm 0,07$	$0,8\pm 0,3$	$0,70\pm 0,08$	$0,77\pm 0,26$
2	$0,73\pm 0,07$	$0,54\pm 0,2$	$0,64\pm 0,07$	$0,57\pm 0,16$
3	$0,79\pm 0,08$	$0,60\pm 0,2$	$0,66\pm 0,07$	$0,62\pm 0,17$
4	$0,80\pm 0,07$	$0,60\pm 0,2$	$0,68\pm 0,06$	$0,64\pm 0,20$
5	$0,79\pm 0,06$	$0,8\pm 0,2$	$0,75\pm 0,06$	$0,78\pm 0,17$

3.3

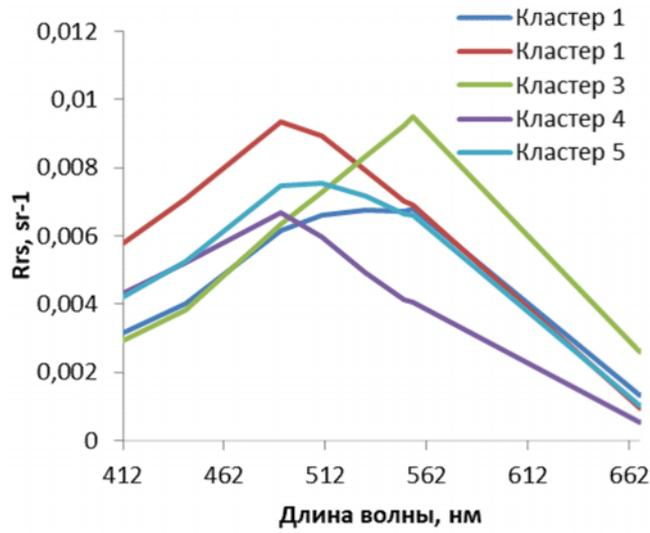
CI(412/443)

0,79.

87%

K-Means)

3.3.



3.3 –

Rrs() 5

5

1

219

540

Rrs()

3.4 ()

130

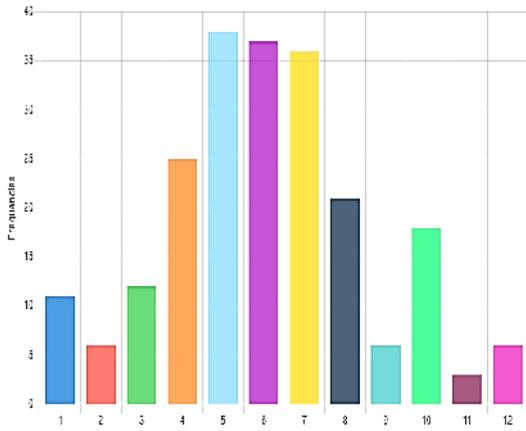
490

3.4. ()

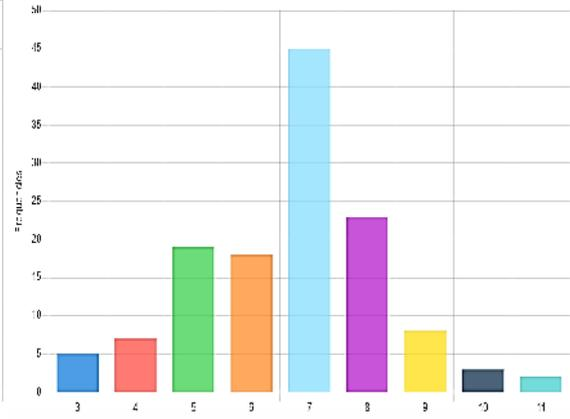
3 (164

565 .

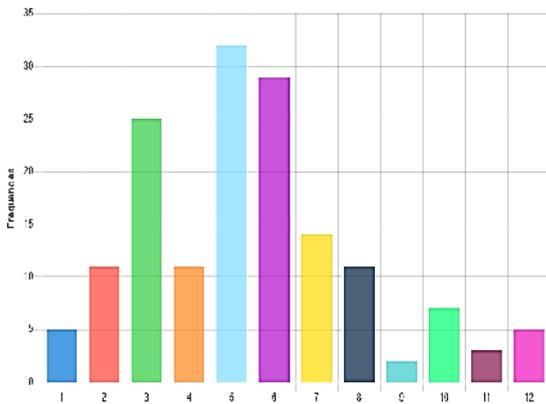
(3.4).



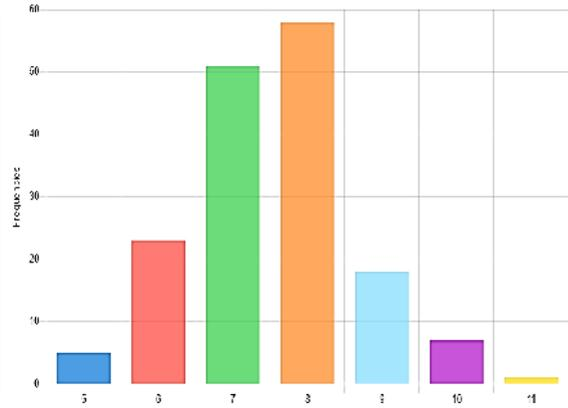
1



2



3



4

3.4 –

1–4

(,).

4

5

, $CI(412/443)$
 $0,81 \pm 0,07$,
 ,
 Rrs(). $CI(412/443)$
 $0,79$ $0,81$ [Shybanov et al., 2022].

3

, (),
 , AERONET-OC (Gloria, Galata).
 , $Rrs()$,
 $in situ$. , 21%

AERONET-OC.

3.2.

(,). ,
 ,
 ,
 . , $CI(412/443)$

$0,80 \pm 0,07$.

.

[..

2022; Shybanov et al., 2022].

4

4.1

, (,)

. - , (,), . .

. , .

(T)

(R)

[Preisendorfer et al., 1976; Plass et al, 1973].

,

$$R, T = \frac{\pi \cdot L}{\mu_0 F_0},$$

$L -$;
 $\mu_0 -$.

, . . .

$$T = \frac{\pi \cdot L_{sc}}{\mu_0 F_0} + \frac{\pi}{\mu_0} \exp[-\tau / \mu_0] \cdot \delta(\mu_0 - \mu) \cdot \delta(\varphi_0 - \varphi),$$

$L_{sc} -$;
 $\tau -$;
 $\delta(x_0 - x) -$;
 $\mu -$;
 $\varphi_0, \varphi -$.

, R T $X,$

$$\hat{X} \cdot L_0 = \frac{1}{\pi} \int_0^1 \int_0^1 X(\mu, \varphi, \mu_0, \varphi_0) \cdot L_0(\mu_0, \varphi_0) \mu_0 d\mu_0 d\varphi_0.$$

, R T ,

, , .

$$\widehat{R} = \widehat{R}_1 + \widehat{T}_1^u \cdot \widehat{R}_2 \cdot \widehat{T}_1^d, \tag{4.1}$$

$$\begin{aligned} R_1 & \text{---} & ; \\ R_2 & \text{---} & ; \\ T^u & \text{---} & ; \\ T^d & \text{---} & . \end{aligned} \tag{4.1}$$

[Shybanov, 2005]

$$R = R_1 + T^u T^d R_2. \tag{4.2}$$

h , $P(h)$, P_0 .
 $z = P(h) / P_0, z \in [0, 1]$.

$$d\tau_m / dz = const = \tau_m^0, \quad \tau_m - h, \quad \tau_m^0 -$$

$$R_2 = \frac{p(\cos \gamma) b(z) dz}{4\mu \mu_0}, \tag{4.3}$$

$b(z) - () z;$

$$p(z, \cos \gamma) = \dots,$$

$$\cos \gamma = -\mu_1 \cdot \mu_2 + \sqrt{1 - \mu_1^2} \sqrt{1 - \mu_2^2} \cos \varphi.$$

$$(4.2) \quad (4.3),$$

$$\frac{dR}{dz} = T^u(z) \cdot T^d(z) \cdot \frac{p(\cos \gamma) \cdot b(z)}{4\mu_0\mu}. \quad (4.4)$$

$$\dots \quad p(\cos \gamma) < 1. \quad T_1 \quad T_2 \quad 1,$$

$$a(z) = \frac{d\tau_a(z)}{dz} \cdot (1 - \Lambda(z)),$$

$$\tau_a(z) =$$

$$z, \Lambda(z) =$$

$$g(z) = \frac{1}{\tau_a^0} \frac{d\tau_a(z)}{dz} = \frac{h_m}{h_a} z^{\frac{h_m - h_a}{h_a}}, \quad \tau_a^0 = \dots, \quad h_m \approx 8 \text{ km}, h_a \approx 1.2 \text{ km} =$$

$$(\dots) =$$

$$T^u(z) = \exp\left[-\frac{1}{\mu_0} \int_0^z a(x) dx\right], T^d(z) = \exp\left[-\frac{1}{\mu_0} \int_0^z a(x) dx\right]. \quad (4.5)$$

$$(4.4)$$

$T:$

$$\frac{dR}{dz} = \frac{p_m(\cos \gamma) \cdot b_m(z)}{4\mu_0\mu} \exp\left[-\left(\frac{1}{\mu_0} + \frac{1}{\mu}\right) \cdot \int_0^z a(x)dx\right] + \frac{p_a(\cos \gamma) \cdot b_a(z)}{4\mu_0\mu} \exp\left[-\left(\frac{1}{\mu_0} + \frac{1}{\mu}\right) \cdot \int_0^z a(x)dx\right],$$

$m, a -$

.

,

, . . .

, $a(z) = 0$

$a(z) \neq 0$

$$r = R(a(z) = 0) - R(a(z) \neq 0).$$

,

.

,

,

.

$$r = \frac{p_m(\cos \gamma) \cdot \tau_m^0(\lambda)}{4\mu_0\mu} a_0(\lambda) \cdot \left(\frac{1}{\mu_0} + \frac{1}{\mu}\right) \int_0^z \int_0^z g(x)dx \cdot dz. \tag{4.6}$$

$$a_0(\lambda) = (1 - \Lambda(\lambda))\tau_a^0 -$$

$$, \tag{4.6}$$

. : 1) g

1 [., 2020], $\int_0^z g(x)dx < 1$

; 2) $(1 - \Lambda(\lambda)) \ll 1$; 3)

$$(1/\mu_0 + 1/\mu)$$

$$a_0(\lambda)$$

$$\frac{p_m(\cos \gamma)}{\mu_0 \mu} \left(\frac{1}{\mu_0} + \frac{1}{\mu} \right) -$$

$$\Lambda(\lambda)$$

[., 2021].

$$a_0(\lambda).$$

$$\tau_m^0(\lambda).$$

$$\tau_m^0 \approx \lambda^{-4}.$$

$$-4.$$

$$\delta = \frac{\tau_m \cdot M_m}{4\mu\mu_0} = \frac{\tau_m}{4\mu\mu_0} \left(1 - \frac{h_a \tau_a^a}{h_a + h_m} \left(\frac{1}{\mu} + \frac{1}{\mu_0} \right) \right). \quad (4.7)$$

AERONET

$$: a_0 = (1 - \Lambda)\tau_a^0.$$

Λ AERONET 4
 (1020 , 870 , 675 , 443), (412 ,
 490 , 532 , 547 , 555 , 667) *Python.*
 (4.7),

c
 ,
 AERONET.

[Penndorf et

al, 1957]

$$\tau_m = \frac{1.545 \cdot 10^{10}}{\lambda^{4.086}}. \tag{4.8}$$

μ_0 , *in situ* AERONET (, Λ, μ
 (4.8) (4.7)
 . ,
 ()

(4.7).

in situ

$$Rrs() (\lambda).$$

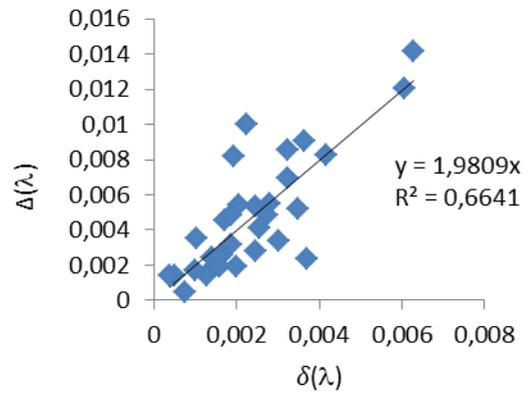
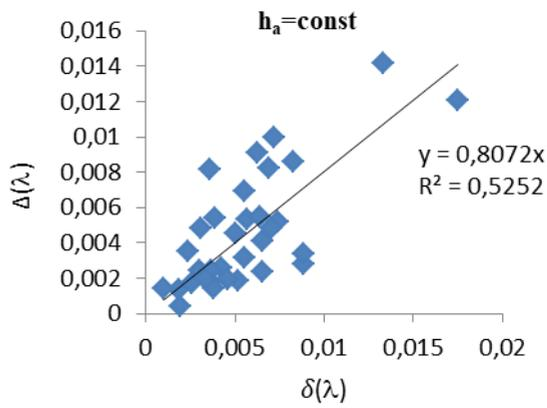
AERONET

MODIS-Aqua.

(PCC) [, 2007]. , 412

0,673 (67%),

(λ)
 h_a 412 (4.1).



()

()

4.1 –

δ

412 () $h_a = \text{const}$ (8) ;

() h_a

h_a

7-

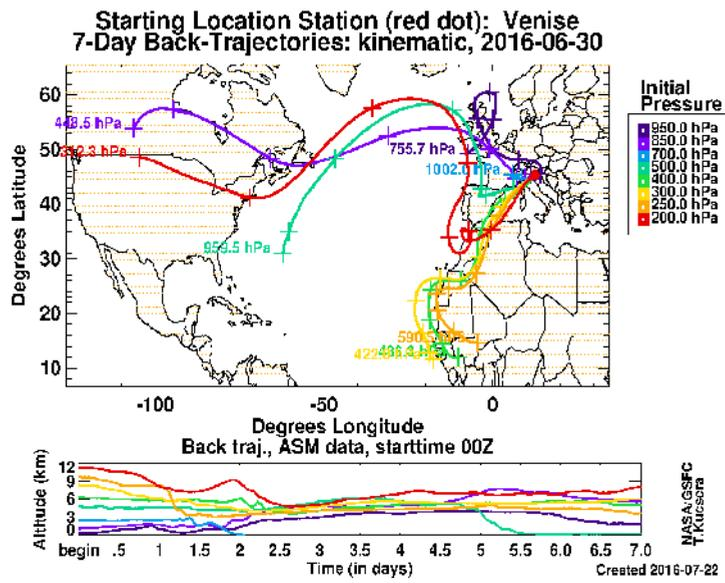
AERONET,

, 30.06.2016 (

)

Venise

6 (4.2).



4.2 –

7-

30.06.2016

()

Venise

().

83%

412

67%

443

10% (412),

(4.1 ()).

(AERONET)

(MODIS-Aqua).

4.2.

()

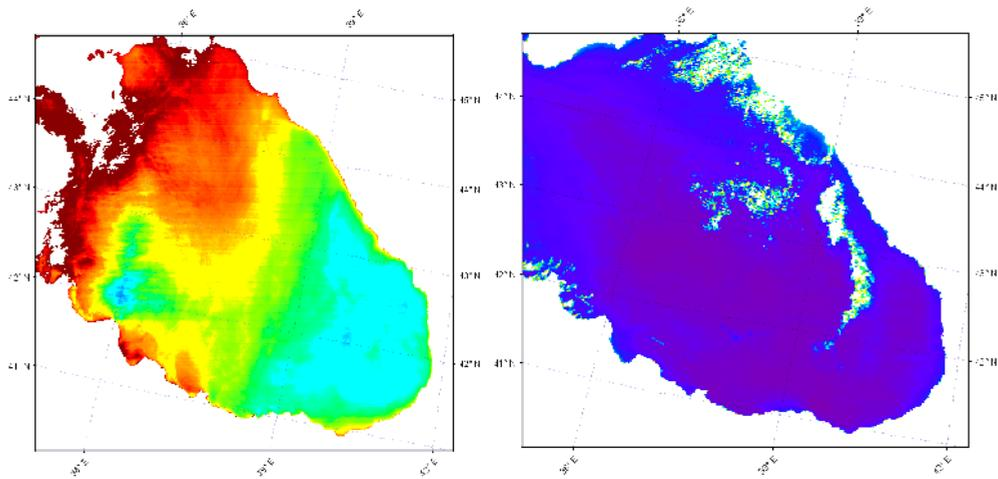
SeaBASS

Rrs()

$Rrs(412) < 0$

(
) [.., 2021] (

4.3) (4.1).



(a)

()

4.3 – $AOT(869)$ ()

MODIS-Aqua

12.09.2017 (a)

08.09.2017 (

)() (

: SeaDAS).

4.1 –

$Rrs()$

(4.3) –

(08.09.2017)

(12.09).

$Rrs()$	412	443	469	488	531	547	555	645	667
08.09	0,0031	0,0040	0,0046	0,0049	0,0039	0,0034	0,0030	0,0004	0,0003
12.09	-0,0002	0,0020	0,0033	0,0036	0,0030	0,0026	0,0023	0,0002	0,0002

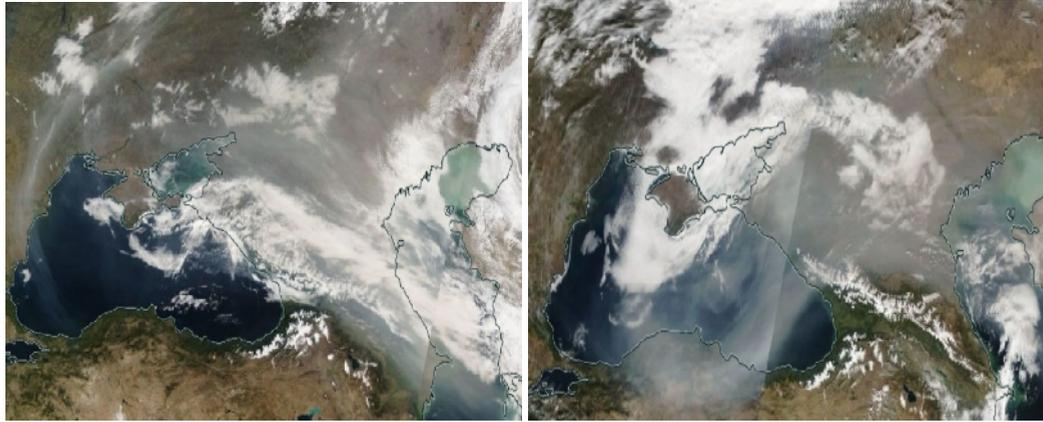
[Kalinskaya et al., 2022].

$Rrs()$

[.., 2022].

19.10.2017

MODIS-Aqua
18–19.10.2017 (4.4).



() ()
 4.4. – MODIS-Aqua :
) 18.10.2017;) 19.10.2017

2017

, 2 :

[Papkova et al., 2022].

(13.10.2017) $Rrs()$
 (19.10.2017).

, $Rrs()$

(13.10.2017) (19.10.2017).

19.10.2017 $Rrs()$

,
 ,
 (4.2).

4.2 –

 $Rrs()$

(13.10.2017)

(19.10.2017)

$Rrs()$	412	443	469	488	531	547	555	645	667
13,10	0,0018	0,0024	0,0029	0,0031	0,0025	0,0022	0,0019	0,0003	0,0003
19,10	-0,0004	0,0022	0,0037	0,0040	0,0041	0,0038	0,0034	0,0017	0,0017

 $Rrs()$

[.., 2021].

 $Rrs()$

AERONET

 $Rrs()$ (MODIS-Aqua).

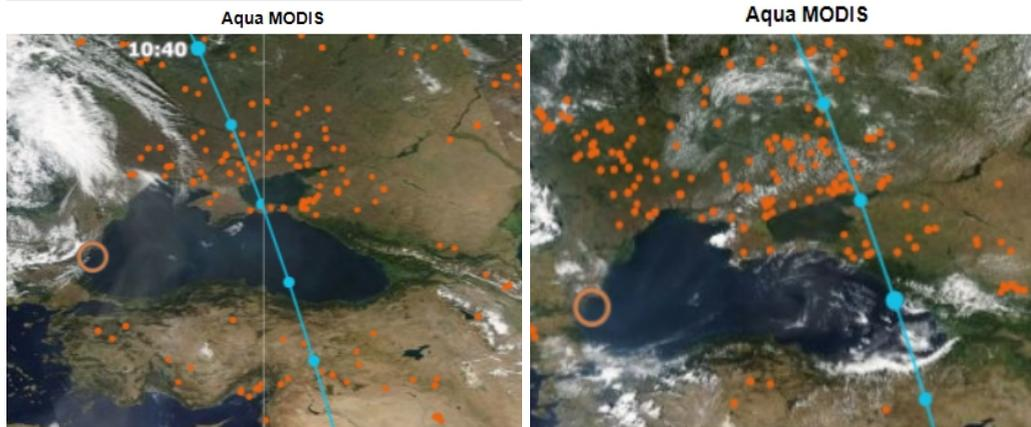
4

:

,

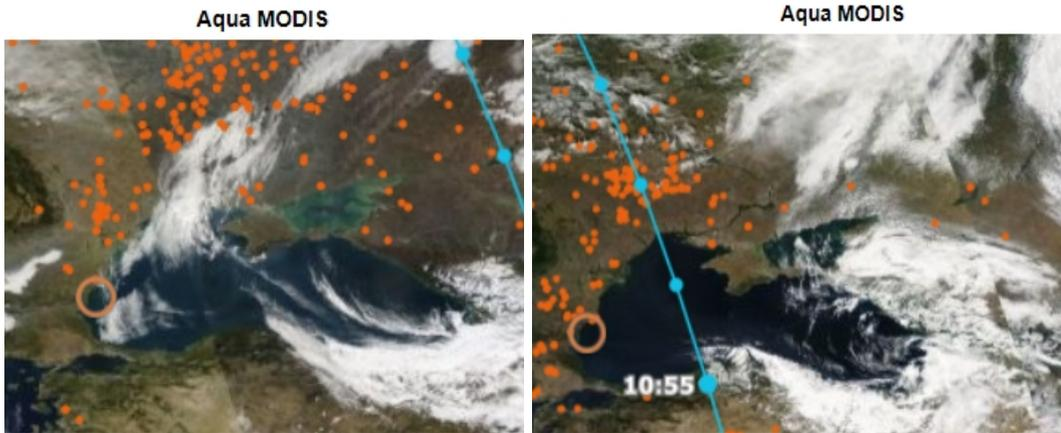
,

(4.5).



11.09.2017 ()

10.08.2016 ()



04.11.2014()

30.09.2016 ()

4.5.

Ocean Color

MODIS-Aqua

in situ

AERONET

(AOT),

(AE),

($\Lambda(z)$).

AOT

, AE

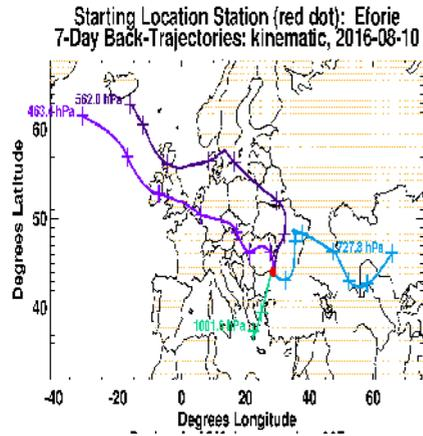
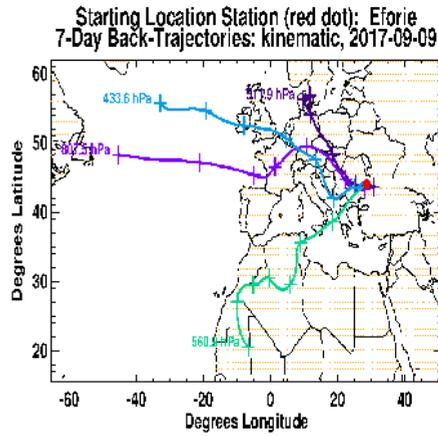
7-

4.6

11.09.2017

(), 10.08.2016

(.).



4.6.

7-

AERONET

09.09.2017

10.08.2016

Eforie ().

AERONET (

3.1)

332

4.3.

4.3 –

MODIS-Aqua

	49
	80
	70
	133
	332

, *in situ* .
, AOT 862 MODIS-Aqua AERONET
72 % ,
37%
(AOT).
in situ ,
(4.4).

4.4 –

(Gloria, Galata)				
AOT				
1020	0,039±0,005	0,040±0,007	0,072±0,01	0,056±0,002
870	0,051±0,007	0,052±0,008	0,091±0,02	0,076±0,008
667	0,077±0,01	0,081±0,02	0,133±0,03	0,111±0,01
551	0,110±0,01	0,116±0,03	0,184±0,05	0,149±0,02
532	0,117±0,03	0,123±0,05	0,195±0,06	0,158±0,02
490	0,132±0,02	0,139±0,03	0,217±0,08	0,185±0,03
443	0,157±0,02	0,163±0,03	0,256±0,08	0,206±0,02
412	0,175±0,03	0,180±0,05	0,283±0,10	0,239±0,05
AE				
440–870	1,688	1,757	1,499	1,541
440–865	1,775	1,730	1,535	1,540

4.4,

2

AE

20–25%

[Li et

al., 2015],

(PCA).

(RMSE),

(R^2)

(

).

$Rrs()$

, PCA

[Pearson, 1901; Fre het, 1948].

in situ

AERONET

MODIS-Aqua.

[, 2022]

$Rrs()$,

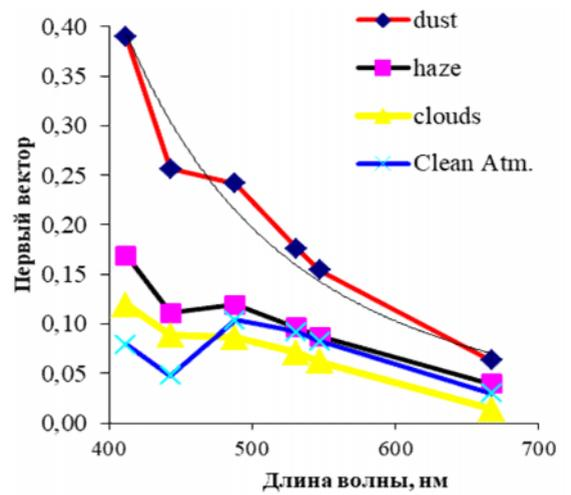
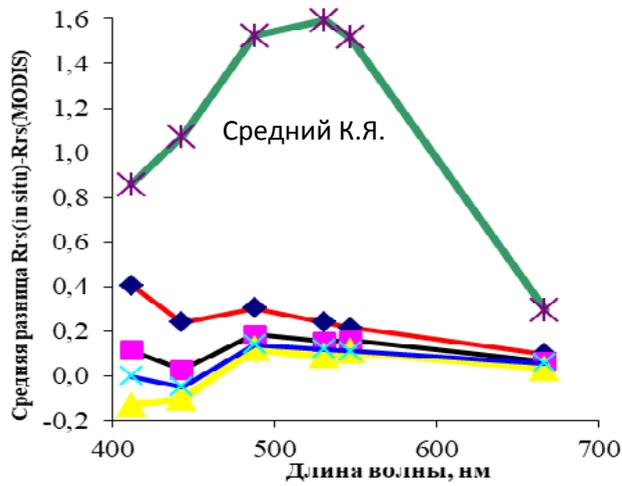
AERONET

PCA

in situ

MODIS-Aqua

4.7.



()

()

4.7. ()

$Rrs()$

MODIS-Aqua

AERONET

; ()

4.7 () ,

Rrs()

PCA

. 4.7 (),

« » ,

4.7 ,

500

4.7 ()

(4.5).

4.5 –

(MODIS-Aqua)

		R^2
	$9 \cdot 10^8 \lambda^{-3,574}$	0,96
	$2 \cdot 10^6 \lambda^{-2,73}$	0,91
	$7 \cdot 10^9 \lambda^{-4,087}$	0,85
	$3 \cdot 10^2 \lambda^{-1,367}$	0,24

4.5,

, R^2

λ^{-4} .

λ (

),

$k=2\pi/\lambda$.

λ^{-4} ,

λ^{-3} .

2022a].

4.3

3.1. 3.2

λ^{-4} .

level 2,

Ocean Color

()

$$Rrs_m(\lambda) = Rrs_{sat}(\lambda) + k \cdot \lambda^{-4}, \tag{4.9}$$

$Rrs_{sat}(\lambda)$ – ,

;

k – .

,

,

$Rrs()$

- [.., 2021; Suslin et al., 2016;

Suslin et al., 2007].

(– 412

) « ,

(

3.2). k

412

,

443

$$k = \frac{CI(\frac{412}{443})Rrs_{sat}(443) - Rrs_{sat}(412)}{(412^{-4} - CI(\frac{412}{443})443^{-4})}. \tag{4.10}$$

, k

, (4.10)

443, 488, 531, 547, 555 667 .

,

AERONET

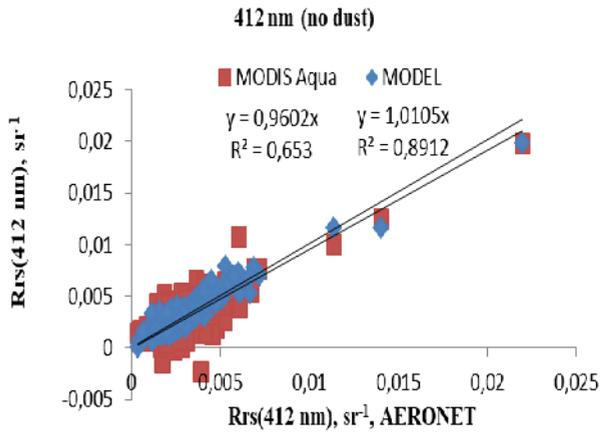
,

(3.1)

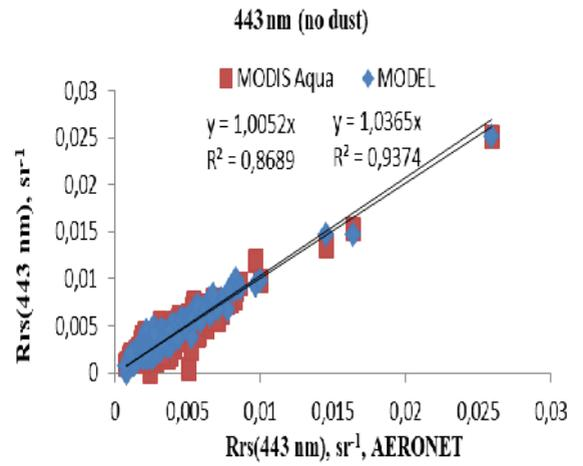
332 .

$Rrs()$

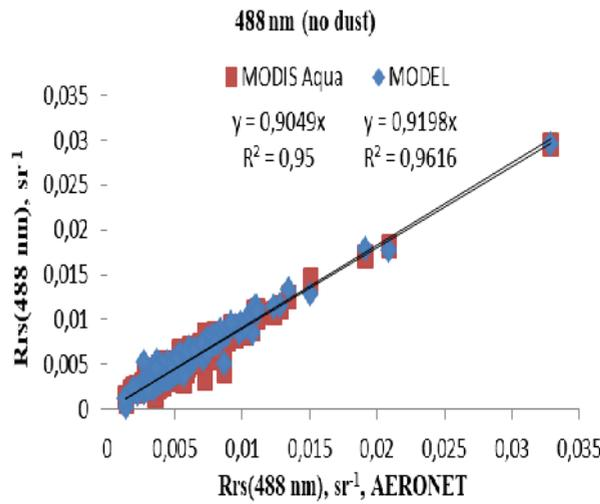
(4.8).



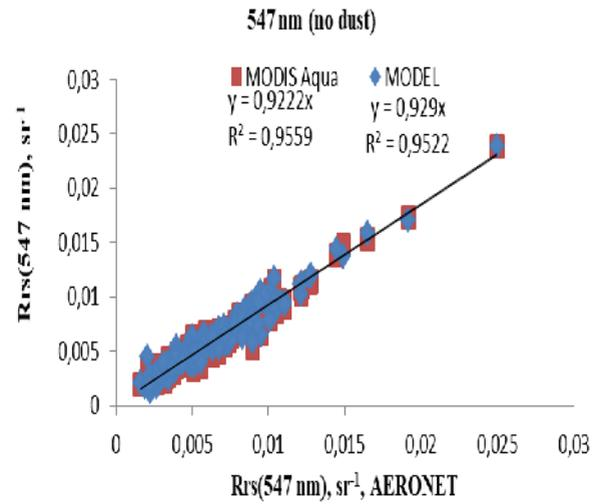
()



()



()



()

4.8 –

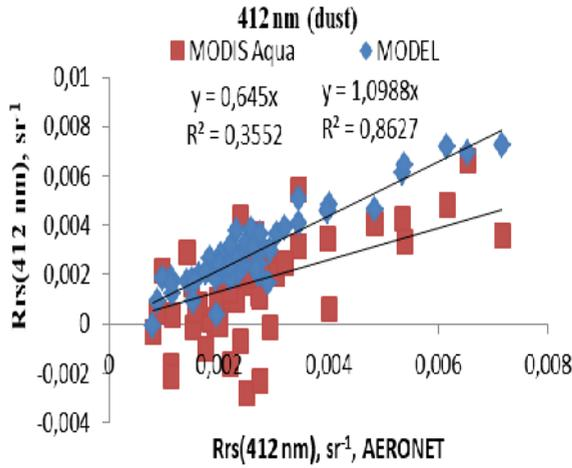
$Rrs()$

MODIS

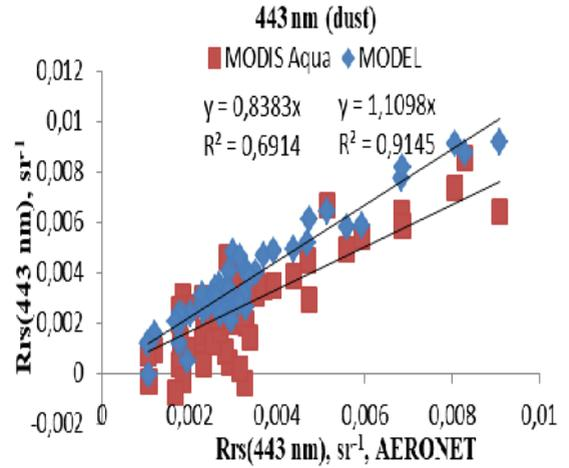
AERONET-OC *in situ*,

412 (), 443 (), 488 (), 547 ()

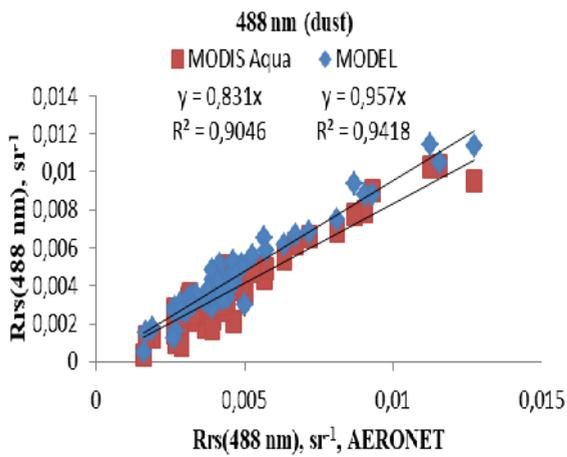
4.9).



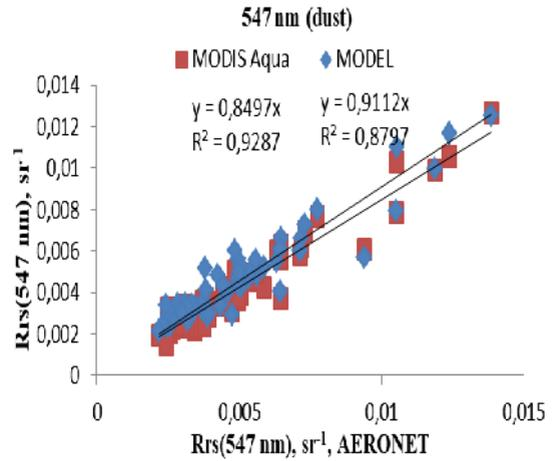
()



()



()



()

4.9 –

$Rrs()$

MODIS

AERONET-OC,

412 (), 443 (), 488 (), 547

()

90

4.8

50 % .

80 %

R^2

2

412

443

531–555

(4.9).

Ocean Color

443

547

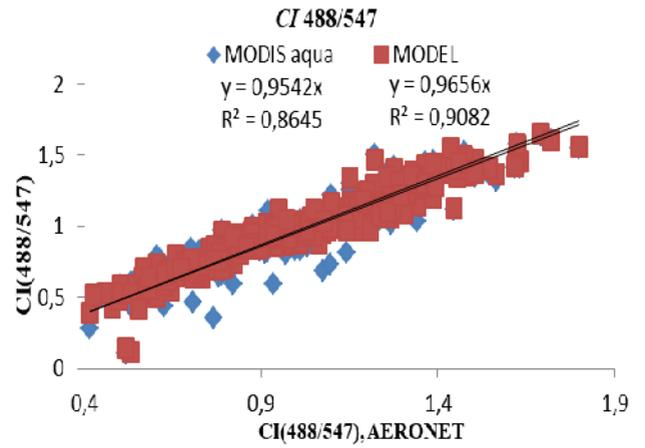
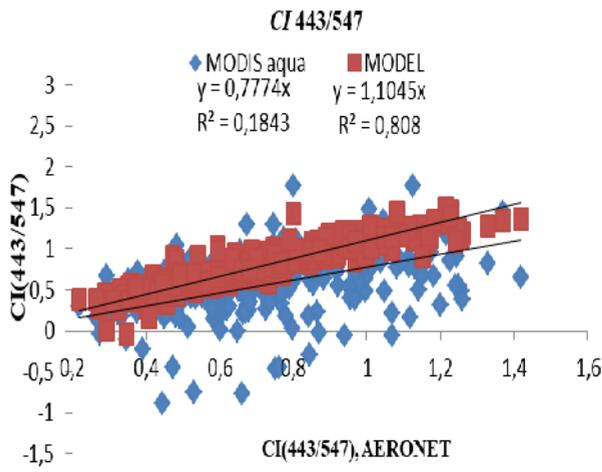
(MODIS-Aqua *OC3M*)

488

547 (MODIS-Aqua *OC2M*).

18%

(), 80% () (4.10).



()

()

4.10 –

CI

MODIS

AERONET-OC,

. 27 2020 .

MODIS-Aqua

869 0,25

412 443

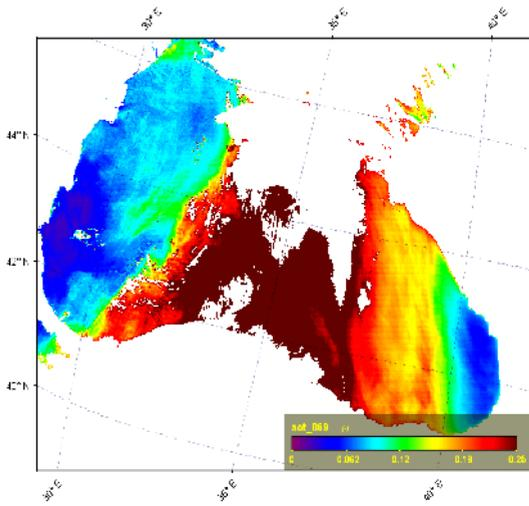
Rrs(),

7 (,)

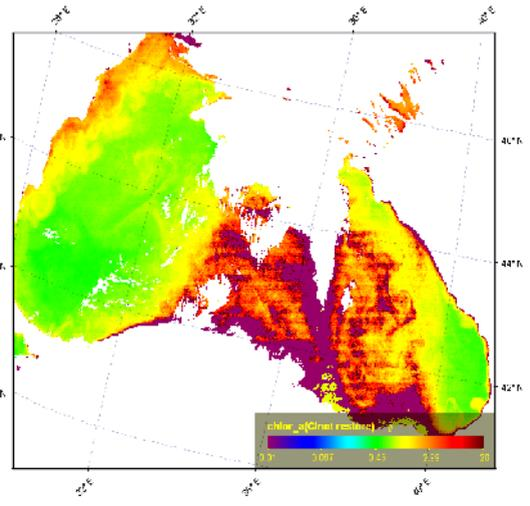
, , , -

7 ()

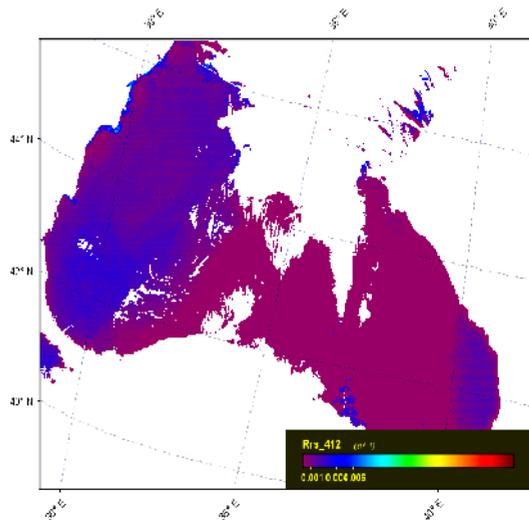
- .



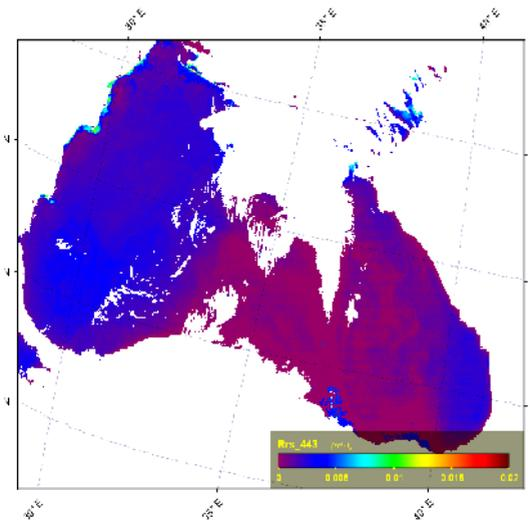
()



()



()



()

4.11 –

MODIS-Aqua 27

2020 .: () , () CI (547/443), () Rrs(412) , () Rrs(443) (SeaDAS)

Rrs()

(

4.12).

4.12 ,

,

,

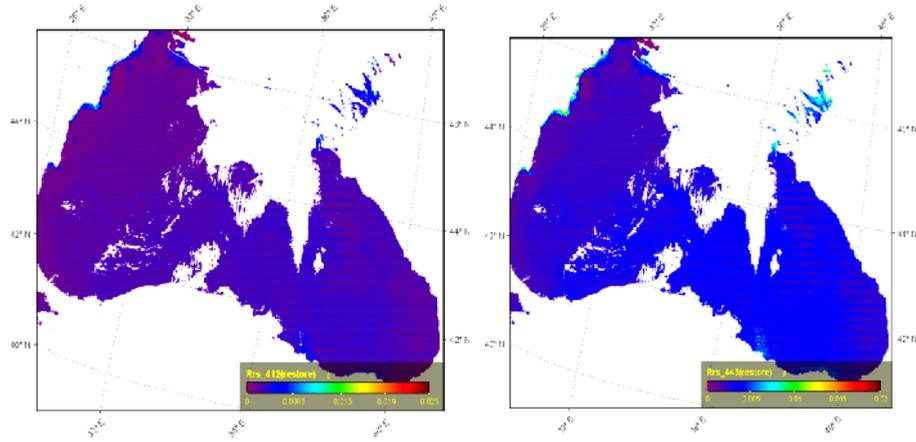
,

.

,

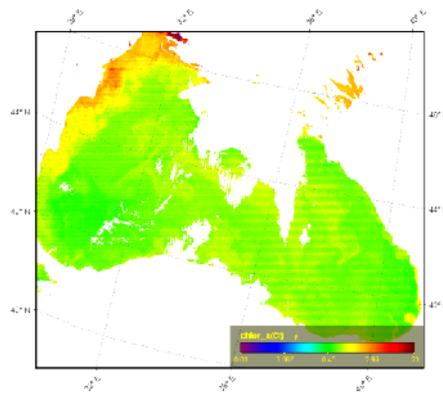
- ,

).



()

()



()

4.12 –

MODIS-Aqua 27

2020 .

: () *Rrs*(412)

, () *Rrs*(443

)

, () *I*(547/443)

(

SeaDAS).

.

,

,

.

,

MODIS-Aqua

12.07.2020

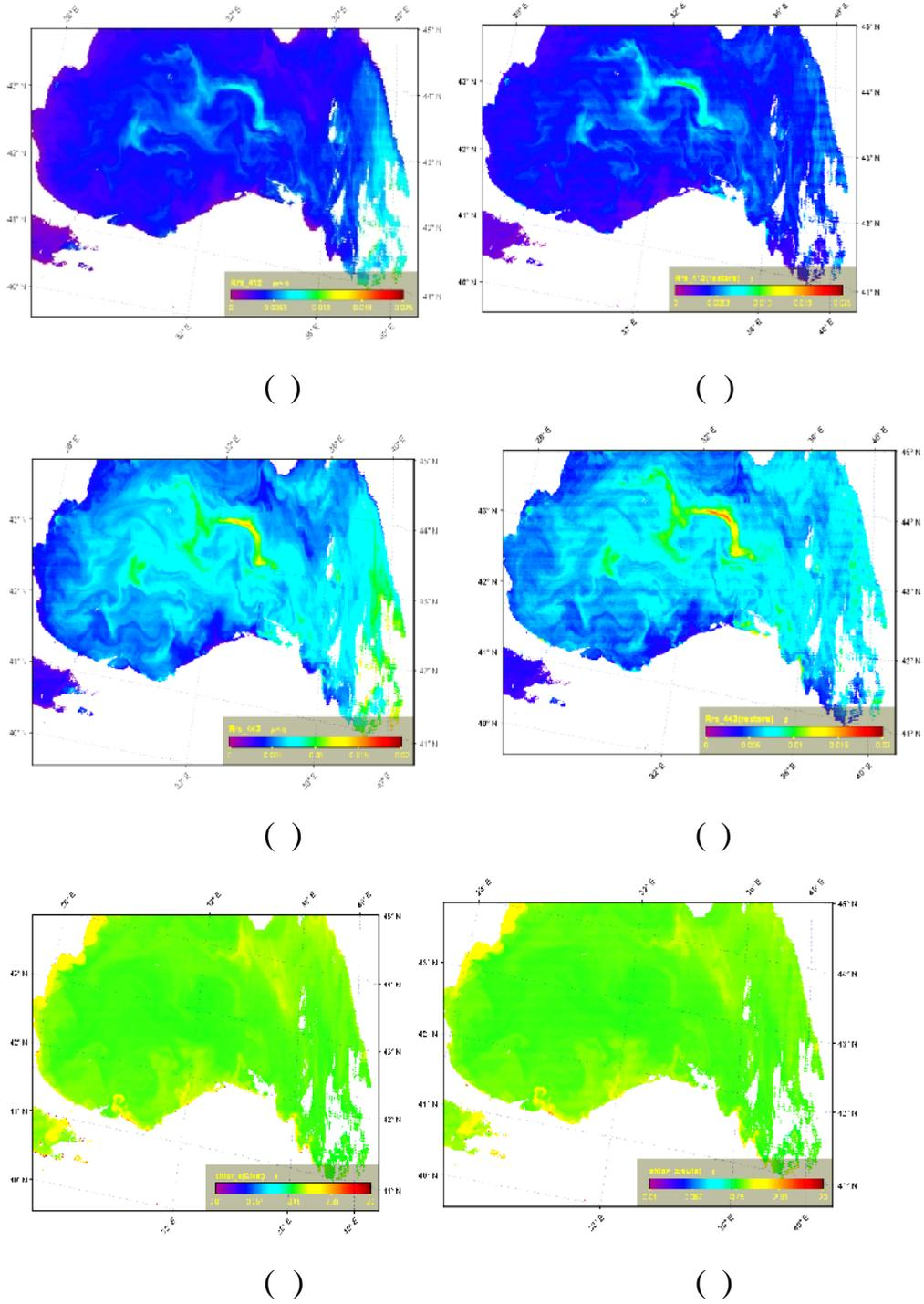
869

(

0,062),

(

. 4.13).



4.13 – MODIS-Aqua 12 2020 .

: () *Rrs*(412) , () *Rrs*(412)
 , () *Rrs*(443) , () *Rrs*(443) ,
 () *CI*(547/443), () *CI*(547/443) (SeaDAS)

(. 4.13).

[Shybanov et al., 2022].

4.4

Rrs *in situ*

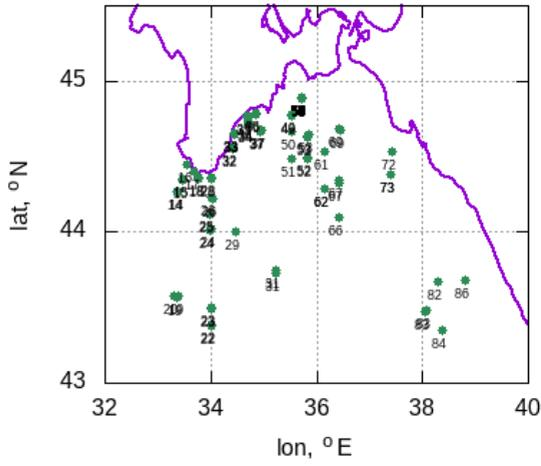
Rrs() , 116 « . ».

2021 . 90 .

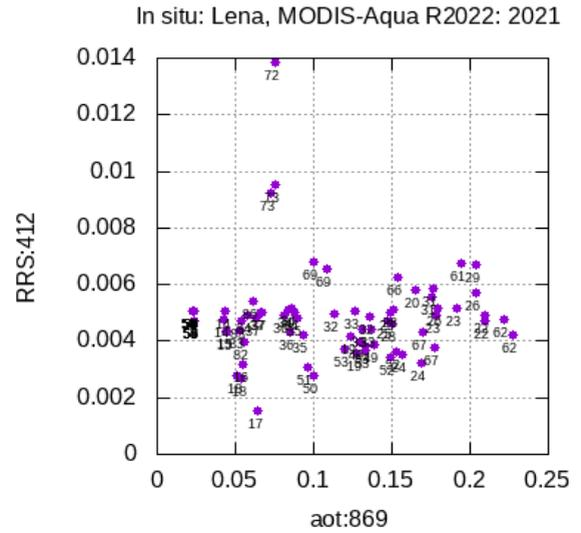
Rrs() [., 2021; Korchemkina et al., 2022]. , *Rrs*() 412 443 0,80±0,03.

, , AERONET- , (3.2).

(*Rrs*() MODIS Aqua Terra. (R2022). *in situ* *Rrs*() 4.14 (). , 4.14 () *Rrs*(412) *Rrs*(412):*Rrs*(443) aot869 (869).



()



()

4.14 – ()

MODIS-Aqua

()

Rrs(412) (869)

: (1)

aot869

0,05 0,25,

(2)

Rrs(412):Rrs(443)

, 0,76.

aot869

4.6.

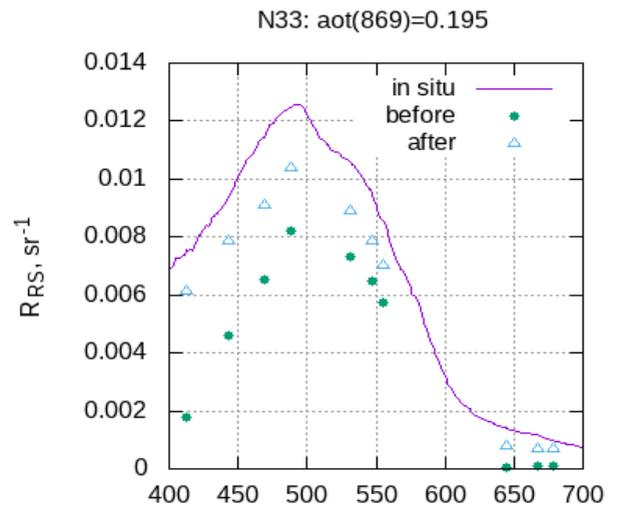
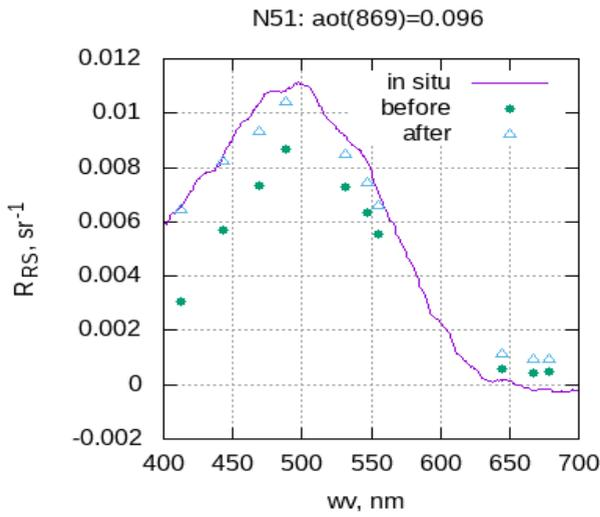
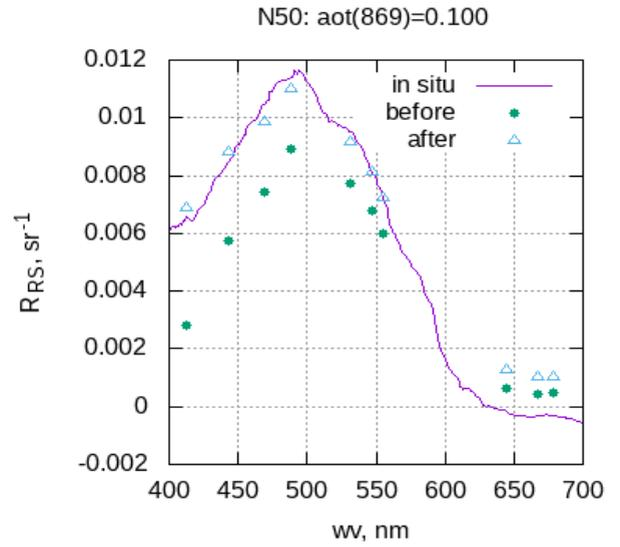
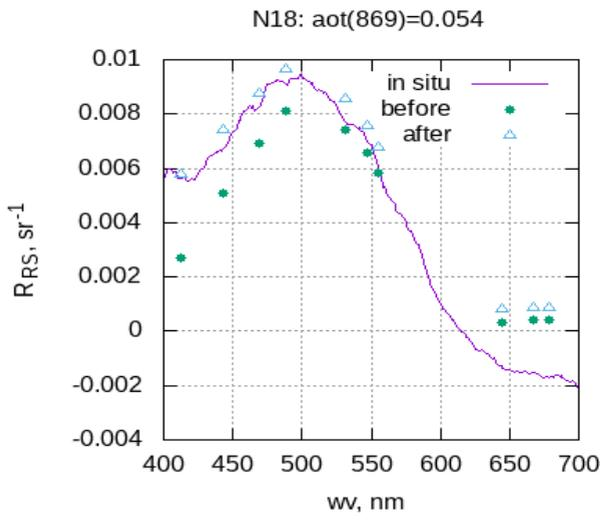
4.6 –

Rrs(),

4.14

	<i>in situ</i>	aot869	
MODIS– Aqua	18	0,054	1,99
MODIS– Aqua	50	0,100	1,46
MODIS– Aqua	51	0,096	1,55
MODIS– Terra	33	0,195	0,58

(4.6) (4.15).



. 4.15.

in situ ()

$R_{rs}(\lambda)$ (before) (after)

4.15 ,

$R_{rs}(\lambda)$

, ,

, , . 4.1 ,
 , ... λ^{-4} .
 .
 ,
 .
 (4.9). ,
 (CI) 412 443 ,
 3.2. ,
 , Rrs(). level 2.
 R^2 Rrs().
 2 412 , 443 488 ,
 531–555 .
 Rrs(). ,
 Chl-a, AERONET
 (60% 412).
 [..
 2022 ; Papkova et al., 2020; .., 2021; , 2022;
 Kalinskaya et al., 2022; Papkova et al, 2022; Shybanov et al., 2022].

100

1.3, , 13%

CI(412/443)

0,80±0,07,

AERONET-OC,

116

«

».

20%.

4.1.

λ^{-4} .

$Rrs()$,

(PCA)

PCA

Rrs

λ

MODIS-Aqua

$$y = 9 \cdot 10^8 \lambda^{-3.574}$$

(4.9).

(CI)

412 443

3.2.

$Rrs()$.

R^2 412 . $Rrs()$ 443 488 ,
 2 531–555 .
 $Rrs()$,
Chl-a, AERONET-OC
 (60% 412).
 116 « . »,

4.4.

,
 (). AERONET
 Ocean Color , *in situ*
 — .
 ,
 , .

L_w – , . -2. -1

L_{TAO} – , . -2. -1

SMA –

SMA –

CZ S – Costal Zone Color Scanner

CDOM –

MODIS – Moderate Resolution Imaging Spectroradiometer

AERONET – Aerosol Robotic Network

– , -1

a_d – , -1

a_{ddm} – , -1

a_{dm} – , -1

a_p – , -1

a_{ph} – -1

a_{ph}^* – , 2. -1

a_w – , -1

b – , -1

b_b – , -1

b_{bw} – , -1

b_{bp} – , -1

c – , -1

C_{ddm} – 400 , -1

chl – (), . -3

h_s –

L – , . -2. -1

Lt –

, . -2. -1

- L_u – , .^{-2.} ⁻¹
- L_{wn} – , .^{-2.} ⁻¹
- CI – ,
- Rrs – , sr⁻¹
- n –
- p – , ^{-1.} ⁻¹
- R – ()
- r –
- F_0 – ,
- t –
- $1, 2$ – ,
- .
- γ –
-
- θ' – , $\theta' = \arcsin(\sin\theta/n)$,
- s –
- ,
- μ_1, μ_2 –
- ρ –
- ρ_{sea} –
- ρ_{surf} –
- ρ_w – ()
- ρ_e –
- ρ_m –
-
- AOT –

τ_r — τ_{Oz} — ϕ —

SSA—

 Rd — , AE — , τ_a^s — , τ_a^a — , h_a — , τ_m — , $h_m \approx 8$ — , $p_a(\mu, \mu_0), p_m(\mu, \mu_0)$ — . p^- ,

— ,

 $strat^-$ C ,

16.
2021;37(2):222–232.
<https://doi.org/10.22449/0233-7584-2021-2-222-232>

17.
SeaWiFS //
. 2004. T. 1. C. 69–79.

18.
SeaWiFS
2002 . //

. 2004. T. 11. . 174–183
19.
//
2001.– . 47–56.

20. . / . .– , 1953. –431

21.
(– 2002)// 2004. 4. . 39–50.

22.
400m / //
. –2008. – 1. – . 38–50.

23.
/ //
" " . –

24. . . . , , ,
 Modis //
 . 2022a. T.35, 7 (402). 532–538 DOI:
 10.15372/AOO20220703
25. . . . ,
 Ocean Color
 //
 .2022. .19. 6, .38-46.
26. *Ahmad, Ziauddin, Bryan A. Franz, Charles R. McClain, Ewa J. Kwiatkowska, Jeremy Werdell, Eric P. Shettle, and Brent N. Holben.* 2010. “New Aerosol Models for the Retrieval of Aerosol Optical Thickness and Normalized Water-Leaving Radiances from the SeaWiFS and MODIS Sensors over Coastal Regions and Open Oceans.” *Applied Optics* 49 (29): 5545
27. *Antoine D.; Morel A.* A multiple scattering algorithm for atmospheric correction of remotely sensed ocean color (MERIS instrument): Principle and implementation for atmospheres carrying various aerosol including absorbing ones. *Int. J. RemoteSens.* 1999, 20, 1875–1916.
28. *Bailey, S.W. and Werdell, P.J.* (2006) A Multi-Sensor Approach for the On-Orbit Validation of Ocean Color Satellite Data Products. *Remote Sensing of Environment*, 102, 12–23. <https://doi.org/10.1016/j.rse.2006.01.015>
29. *Balch W.M., Bowler B.C., Drapeau D.T, Lubelczyk L.C, Lyczkowski E.* Vertical distributions of Coccolithophores, PIC, POC, Biogenic Silica, and Chlorophyll a throughout the Global Ocean *Glob. Biogeochem. Cycles*, 32 (2018), pp. 2–17,
30. *Balch W.M., Drapeau D.T, Bowler B.C., Lyczkowski E, Booth E.S.* The contribution of coccolithophores to the optical and inorganic carbon budgets during the Southern Ocean Gas Exchange Experiment: new evidence in support of the Great Calcite Belt hypothesis *J. Geophys. Res. Ocean*, 116 (2011), pp. 1–14, 10.1029/2011JC006941

31. *Basart, S. and Pérez, C. and Cuevas, E. and Baldasano, J. M. and Gobbi, G. P.* Aerosol characterization in Northern Africa, Northeastern Atlantic, Mediterranean Basin and Middle East from direct-sun AERONET observations, 2009, *Atmos. Chem. Phys.*, V.9, pp. 8265—8282
32. *Bricaud, A., Babin, M., Morel, A., Claustre.* Variability in the chlorophyll-specific absorption coefficients of natural phyto-plankton: Analysis and parameterization, *J. Geophys. Res.*, 1995, Vol. 100, pp. 13321–13332. DOI : 10.1029/95JC00463
33. *Brown C.W., Yoder J.A.* Coccolithophorid blooms in the global ocean *J. Geophys. Res.*, 99 (1994), pp. 7467–7482, 10.1029/93JC02156
34. *Chomko, R.; Gordon, H.R.* Atmospheric correction of ocean color imagery: Use of the Junge power-law aerosol size distribution with variable refractive index to handle aerosol absorption. *Appl. Opt.* 1998, 37, 5560–5572
35. *Cokacar T., Kubilay N , Oguz T.* Structure of *Emiliana huxleyi* blooms in the Black Sea surface waters as detected by Sea WIFS imagery *Geophys. Res. Lett.*, 28 (2001), pp. 4607–4610, 10.1029/2001GL013770
36. *Davies C. N.* Size distribution of atmospheric particles, *J. Aerosol Sci.* 5, 293–300 (1974)
37. *Deirmendjian D.*, Scattering and polarization properties of water clouds and hazes in the visible and infrared, *Appl. Opt.* 3, 187–196 (1964).
38. *Dubovik, O. and M. D. King,* A flexible inversion algorithm for retrieval of aerosol optical properties from Sun and sky radiance measurements, *J. Geophys. Res.*, 105, 20,673–20,696, 2000.
39. *Dubovik, O., A. Smirnov, B.N. Holben, M.D. King, Y. J. Kaufman, T.F. Eck and I. Slutsker,* Accuracy assessment of aerosol optical properties retrieval from AERONET sun and sky radiance measurements, *J. Geophys. Res.* 105, 9791–9806, 2000
40. *Fre het M.* Les éléments aléatoires de nature quelconque dans un espace distancié. *Ann. Inst. H. Poincaré*, 10 (1948), 215–310.

41. *Frouin, R., Duforêt, L., and Steinmetz, F.* (2014). "Atmospheric correction of satellite ocean–color imagery in the presence of semi–transparent clouds," in Proceedings SPIE (Beijing), 926108.
42. *Gkikas, A., Proestakis, E., Amiridis, V., Kazadzis, S., Di Tomaso, E., Tsekeri, A., Marinou, E., Hatzianastassiou, N., and Pérez García–Pando, C.:* *ModIs . Dust AeroSol (MIDAS): a global fine–resolution dust optical depth data set*, *Atmos. Meas. Tech.*, 14, 309–334, <https://doi.org/10.5194/amt-14-309-2021>, 2021.
43. *Gordon H.R.* Can the Lambert–Beer law be applied to the diffuse attenuation coefficient of ocean water // *Limnology and Oceanography*. 1989. V. 34. No. 8. P. 1389–1409.
44. *Gordon, H. R.* (1978). Removal of atmospheric effects from satellite imagery of the oceans. *Appl. Opt.* 17:1631. doi: 10.1364/AO.17.001631
45. *Gordon, H. R., Wang, W.* (1994). Influence of oceanic whitecaps on atmospheric correction of SeaWiFS. *Applied Optics* 33(33), 7754–7763. doi:10.1364/ao.33.007754
46. *Gordon, H.R.; Du, T.; Zhang, T.* Remote sensing of ocean color and aerosol properties: Resolving the issue of aerosol absorption. *Appl. Opt.* 1997, 36, 8670–8684
47. *Hänel G.* The properties of atmospheric aerosol particles as functions of the relative humidity at thermodynamic equilibrium with the surrounding moist air, *Advances in Geophysics*, H. E. Landsberg and J. V. Miehem, eds. (Academic, 1976), Vol. 19.
48. *Holben B.N., Eck T.F., Slutsker I., Tanré D., Buis J.P., Setzer A., Vermote E., Reagan J.A., Kaufman Y.J., Nakajima T., Lavenue F., Jankowiak I., Smirnov A.,* AERONET—A Federated Instrument Network and Data Archive for Aerosol Characterization, *Remote Sensing of Environment*, Volume 66, Issue 1, 1998, Pages 1–16.
49. *Howard R, Gordon and Menghua Wang,* "Retrieval of water–leaving radiance and aerosol optical thickness over the oceans with SeaWiFS: a preliminary algorithm," *Appl. Opt.* 33, 443–452 (1994)

50. *Hu C., Feng L., Lee Z., Franz B. A., Bailey S. W., Werdell P. J., & Proctor C. W.* (2019). Improving satellite global chlorophyll a data products through algorithm refinement and data recovery. *Journal of Geophysical Research: Oceans*, 124(3), 1524–1543, doi: [10.1029/2019JC014941](https://doi.org/10.1029/2019JC014941)
51. *Hu C., Lee Z., & Franz B.* (2012). Chlorophyll a algorithms for oligotrophic oceans: A novel approach based on three–band reflectance difference . *Journal of Geophysical Research*, 117(C1).
52. *Iglesias–Rodríguez M.D., Brown C.W., Doney S.C., Kleypas J., Kolber D. Z. et al.* Representing key phytoplankton functional groups in ocean carbon cycle models: coccolithophorids *Glob. Biogeochem. Cycl.*, 16 (2002), [10.1029/2001gb00145447-1-47-20](https://doi.org/10.1029/2001gb00145447-1-47-20)
53. IOCCG (2000) Remote sensing of ocean colour in coastal, and other optically–complex, waters. Sathyendranath, S. (ed.), Reports of the International Ocean–Colour Coordinating Group, No. 3, IOCCG, Dartmouth, Canada. – 140 p
54. IOCCG (2006). “Remote sensing of inherent optical properties: fundamentals, tests of algorithms, and applications,” in Report No. 5 of the International Ocean–Colour Coordinating Group, ed Z. Lee (Dartmouth, NS: IOCCG), 126.
55. IOCCG (2007). “Ocean–colour data merging,” in Report No. 6 of the International Ocean–Colour Coordinating Group, ed W. W. Gregg (Dartmouth, NS: IOCCG), 68.
56. IOCCG (2008). “Why ocean colour? the societal benefits of ocean–colour technology,” in Report No. 7 of the International Ocean–Colour Coordinating Group, eds T. Platt, N. Hoepffner, V. Stuart, and C. Brown (Dartmouth, NS: IOCCG), 141.
57. IOCCG (2010). “Atmospheric correction for remotely–sensed ocean–colour products,” in Reports No. 10 of the International Ocean–Colour Coordinating Group, ed M. Wang (Dartmouth, NS: IOCCG), 78.
58. IOCCG (2012). “Mission requirements for future ocean–colour sensors,” Report No. 13 of the International Ocean–Colour Coordinating Group, eds McClain and Meister (Dartmouth, NS: IOCCG), 106.

59. IOCCG (2013). “In-flight calibration of satellite ocean-colour sensors,” Report No. 14 of the International Ocean-Colour Coordinating Group, ed R. Frouin (Dartmouth, NS: IOCCG), 106.
60. IOCCG (2014). “Phytoplankton functional types from space,” Report No. 15 of the International Ocean-Colour Coordinating Group, ed S. Sathyendranath (Dartmouth, NS: IOCCG), 156.
61. *Jamet, C., Moulin, C., and Thiria, S.* (2004). Monitoring aerosol optical properties over the Mediterranean from SeaWiFS images using a neural network inversion. *Geophys. Res. Lett.* 31:L13107. doi: 10.1029/2004GL019951
62. *Junge C. E.* Our knowledge on the physico-chemistry of aerosols in the undisturbed marine environment, *J. Geophys. Res.* V. 77, 5183–5200 (1972).
63. *Kalinskaya, D., Papkova, A., Papkova, Y., Gurov, K.* Quality assessment of the aerosol optical depth by AERONET, MODIS and CALIPSO over the western part of the Black sea region // International Multidisciplinary Scientific GeoConference Surveying Geology and Mining Ecology Management, SGEM. 2019. T.19, 4.1. 1041-1046
64. *Kalinskaya, D.V., Papkova, A.S.* Optical characteristics of atmospheric aerosol from satellite and photometric measurements at the dust transfers dates // Proceedings of SPIE - The International Society for Optical Engineering. 2020. T.11560, 115603S
65. *Kalinskaya, D.V., Papkova, A.S.* Effect of the absorbing aerosol on the value of the brightness spectral factor by AERONET data and MODIS satellite data over the Black sea region // Proceedings of SPIE - The International Society for Optical Engineering. 2019. T.11208, 112084R
66. *Kalinskaya, D.V., Papkova, A.S.* Identification of the marine aerosol by the CALIPSO radiometer over the Black sea for 2017 // Proceedings of SPIE - The International Society for Optical Engineering. 2018. T.10833, UNSP 108335K
67. *Kalinskaya, D.V., Papkova, A.S.* Influence of dust transfers on aerosol asymmetry factor over the Black Sea region according to AERONET data // Proceedings of SPIE - The International Society for Optical Engineering. 27th International

Symposium on Atmospheric and Ocean Optics, Atmospheric Physics
2021Moscow5 July 2021 9 July 2021. 2021. T.11916, . 1191645

68. *Kalinskaya, D.V.; Papkova, A.S.* Why Is It Important to Consider Dust Aerosol in the Sevastopol and Black Sea Region during Remote Sensing Tasks? A Case Study. *Remote Sens.* **2022**, *14*, 1890.
69. *Kim, M.H., Omar, A. H., Tackett, J. L., Vaughan, M. A., Winker, D. M., Trepte, C. R., Hu, Y., Liu, Z., Poole, L. R., Pitts, M. C., Kar, J., and Magill, B. E.:* The CALIPSO version 4 automated aerosol classification and lidar ratio selection algorithm, *Atmos. Meas. Tech.*, *11*, 6107–6135, 2018.
70. *Kopelevich O.V., Burenkov V.I., Sheberstov S.V., Vazyulya S.V., Kravchishina M.D., Pautova L., Silkin V.A., Artemiev V.A., Grigoriev V.* Satellite monitoring of coccolithophore blooms in the Black Sea from ocean color data // *Remote Sensing of Environment*. 2014. V. 146. P. 113–123.
71. *Korchemkina E.N., Kalinskaya D.V.* Algorithm of additional correction of level 2 remote sensing reflectance data using modelling of the optical properties of the black sea waters. *Remote Sensing*. 2022. . 14. 4.
72. *Kubryakov A.A., Mikaelyan A.S., Stanichny S. V.* Summer and winter coccolithophore blooms in the Black Sea and their impact on production of dissolved organic matter from Bio–Argo data // *Journal of Marine Systems*. 2019. Vol. 199. 103220.
73. *Lee J, Hsu NC, Sayer AM, Bettenhausen C, Yang P.* AERONET–based nonspherical dust optical models and effects on the VIIRS Deep Blue/SOAR over–water aerosol product. *J Geophys Res Atmos.* 2017 Oct 16;122(19):10384–10401. doi: 10.1002/2017jd027258.
74. *Li J., Carlson B. E. and Lacis A. A.* (2015), Using single–scattering albedo spectral curvature to characterize East Asian aerosol mixtures. *J. Geophys. Res. Atmos.*, *120*: 2037– 2052. doi:10.1002/2014JD022433.
75. *Lobkov, V.A.* Odessa region of the Black Sea: hydrobiology of the pelagic and benthal. *IMB Monographies* 2017,p.320.

76. *Mikaelyan A.S., Pautova L.A., Pogosyan S.I., Sukhanova I.N.* Summer bloom of coccolithophorids in the northeastern Black Sea // *Oceanology*. 2005. . 45. . S127.
77. *Mikaelyan A.S., Silkin V.A., Pautova L.A.* Coccolithophorids in the Black Sea: their interannual and long-term changes // *Oceanology*. 2011. . 51. . 1. . 39–48.
78. *Mitchell C., Hu C., Bowler B., Drapeau D., Balch W.M.* Estimating particulate inorganic carbon concentrations of the global ocean from ocean color measurements using a reflectance difference approach *J. Geophys. Res. Ocean*, 122 (2017), pp. 8707–8720, 10.1002/2017JC013146
79. *Mobley C. D.* Phase function effects on oceanic light fields / C.D. Mobley, L.K. Sundman, E. Boss // *Appl. Opt.* – 2002. – Vol. 41. – . 1035–1050.
80. *Mobley, C. D., Werdell, J., Franz, B., Ahmad, Z., and Bailey, S.:* Atmospheric Correction for Satellite Ocean Color Radiometry, National Aeronautics and Space Administration, Washington, DC, USA, <https://oceancolor.gsfc.nasa.gov/docs/technical/NASA-TM-2016-217551.pdf> (last access: 18 August 2022), 2016.(4):
81. *Morel A, Voss Kj, Gentili B.* Bidirectional reflectance of oceanic waters – a comparison of modeled and measured upward radiance fields. *Journal of Geophysical Research. Oceans*, 1995, 100 (C7), pp.13143–13150.
82. *Morel A., Prier L.* Analysis of variations in ocean color // *Limnol. Oceanogr.* 1977. V. 22. No. 4. P. 709–722.
83. *Morel, A.; Prieur, L.* Analysis of variations in ocean color. *Limnol. Oceanogr.* 1977, 22, 709–722.
84. *Müller M.N.* On the genesis and function of coccolithophore calcification *Front. Mar. Sci.*, 6 (2019), p. 49, 10.3389/fmars.2019.00049
85. *O'Reilly, J.E. and Werdell, P.J.* (2019) Chlorophyll algorithms for ocean color sensors – OC4, OC5 & OC6. *Remote Sensing of Environment*, 229, pp.32–47. DOI: <https://doi.org/10.1016/j.rse.2019.04.021>.
86. *O'Reilly, J.E., Maritorena, S., Mitchell, B. G., Siegel, D. A., Carder, K. L., Garver, S. A., Kahru, M., & McClain, C. R.* (1998). Ocean color chlorophyll algorithms for

SeaWiFS, *Journal of Geophysical Research* 103, 24937–24953, doi: 10.1029/98JC02160.

87. *Papkova A. S., Kalinskaya D. V., Shybanov E. B.*, "Atmospheric correction according to the MODIS and VIIRS satellite data with considering the atmospheric pollution factor by a combination of different types of aerosol," 2022. Proc. SPIE 12341, 28th International Symposium on Atmospheric and Ocean Optics: Atmospheric Physics, 123414G
88. *Papkova A., Papkova Y., Shukalo D.* Modelling episode of Saharan dust transfer over the Black Sea according to the WRF model and MODIS satellite data E3S Web Conf., 285 (2021) 08004
89. *Papkova, A., Papkov, S., Shukalo, D.* Modelling the generation of dusty marine aerosol by expeditionary data and remote sensing methods over the Black Sea region // E3S Web of Conferences. 2020. T.224, . 02031
90. *Pearson K.*, On lines and planes of closest fit to systems of points in space, *Philosophical Magazine*, (1901) 2, 559—572;
91. *Penndorf R.*, "Tables of the Refractive Index for Standard Air and the Rayleigh Scattering Coefficient for the Spectral Region between 0.2 and 20.0 μ and Their Application to Atmospheric Optics," *J. Opt. Soc. Am.* 47, 176–182 (1957).
92. *Plass G.N.* Matrix Operator Theory II. Scattering from Maritime Haze G.N. Plass, G.W Kattawar., F.E. Catchings // *Appl. Opt.* – 1973. – Vol. 12. – P. 1071–1084.
93. *Preisendorfer R.W.* Hydrologic Optics / R.W. Preisendorfer // VOLUME II, Chapter 3, The Interaction Principle, Joint Tsunami Research Effort, Honolulu Hawaii, U.S. Department of Commerce, NOAA, Environmental Research Laboratories, Pacific Marine Environmental Laboratory, 1976. – P. 188–400.
94. *Ruddick K.G., Voss K, Boss E, Castagna A, Frouin R, Gilerson A, Hieronymi M, Johnson BC, Kuusk J, Lee Z, Ondrusek M, Vabson V, Vendt R.* A Review of Protocols for Fiducial Reference Measurements of Water–Leaving Radiance for Validation of Satellite Remote–Sensing Data over Water. *Remote Sensing*. 2019; 11(19):2198. <https://doi.org/10.3390/rs11192198>

95. *Schoeberl, M. R., and P. A. Newman*, A multiple-level trajectory analysis of vortex filaments, *J. Geophys. Res.*, 100, 25,801–25,816, 1995
96. *Shettle, E. P., Fenn, R. W.* (1976) Models of the Atmospheric Aerosols and their Optical Properties, in AGARD Conference Proceedings No. 183 Optical Propagation in the Atmosphere AGARD-CP-183, available from the U.S. National Technical Information Service, AD A028-615.
97. *Shibanov E.B.* Numerical method for the solution of the equation of radiation transfer. Reflection and transmission coefficients for an optically thin plane-parallel layer / E.B. Shibanov // *Physical Oceanography*. – 2005. – V. 15, Issue 3. – P. 192–202. doi: 10.1007/s11110-005-0041-2.
98. *Smith R.C.* Optical properties of clearest natural waters (200–800 nm) // *Appl. Optics*. 1981. V. 20. P. 177–184.
99. *Sosik H.M.* Light absorption by phytoplankton, photosynthetic pigments and detritus in California Current System / H.M. Sosik, B.G. Mitchell // *Deep-Sea Res.* – 1995. – Vol. 42. – 10. – P. 1717–1748.
100. *Suslin, V.V.; Slabakova, V.K.; Kalinskaya, D.V.; Pryakhina, S.F.; Golovko, N.I.* Optical features of the Black Sea aerosol and the sea water upper layer based on in situ and satellite measurements. *Phys. Oceanogr.* **2016**, *1*, 20–32.
101. *Suslin, V.V.; Suetin, V.S.; Korolev, S.N.; Kucheryaviy, A.A.* Desert dust effects in the results of atmospheric correction of satellite sea color observations. In Proceedings of the 4th International Conference on Current Problems in Optics of Natural Waters, Nizhny Novgorod, Russia, 11–15 September 2007; pp. 184–187
102. *Shybanov E.B. and Papkova A.S.*, Algorithm for Additional Correction of Remote Sensing Reflectance in the Presence of Absorbing Aerosol: Case Study // *PHYSICAL OCEANOGRAPHY*. 2022. . 29(6). . 688-706. doi:10.22449/1573-160X-2022-6-688-706
103. *Sylvester J.J.*, On the reduction of a bilinear quantic of the nth order to the form of a sum of n products by a double orthogonal substitution, *Messenger of Mathematics*, 19 (1889), 42–46.

104. *Thuillier, G., Hersé, M., Labs, D., et al.* (2003). The solar spectral irradiance from 200 to 2400 nm as measured by the SOLSPEC spectrometer from the Atlas and Eureka missions. *Solar Physics* 214: 1. doi:10.1023/A:1024048429145
105. *Viollier M.* An algorithm for remote sensing of water color from space / M. Viollier , D. Tanre, P.Y. Deschamps // *Boundary–Layer Meteorol.* – 1980. – Vol.18. – No.3. – P. 247–267
106. *Werdell P.J., Bailey S.W.* The SeaWiFS Bio–Optical Archive and Storage System (SeaBASS): Current Architecture and Implementation // NASA /TM 2002–211617. Goddard Space Flight Center. Greenbelt, Maryland. 2002.
107. *Werdell P.J., Bailey S.W.* The SeaWiFS Bio–Optical Archive and Storage System (SeaBASS): Current Architecture and Implementation // NASA /TM 2002–211617. Goddard Space Flight Center. Greenbelt, Maryland. 2002.
108. *Whitby, K. T., Cantrell, B.* (1975) Atmospheric aerosols – Characteristics and measurements, International Conf. on Environmental Sensing and Assessment, 2, Las Vegas, Nev., 14–19 September 1975
109. *William D. Philpot,* Radiative transfer in stratified waters: a single–scattering approximation for irradiance, *Appl. Opt.* 26, 4123–4132 (1987)
110. *Zibordi G., Mélin F., Berthon J.F., Talone M.* In situ autonomous optical radiometry measurements for satellite ocean color validation in the Western Black Sea *Ocean Sci.*, 11 (2015), pp. 275–286, 10.5194/os-11-275-2015
111. *Zibordi, G., Holben, B., Slutsker, I., Giles, G., D’Alimonte, D., Melin, F., Berthon, Vandemark J. F., Feng D., Schuster H., Fabbri G., Kaitala B. E., Seppala J.* (2009). AERONET–OC: A Network for the Validation of Ocean Color Primary Products. *J. Atmos. and Oceanic Technology.* 26, 1634–1651.